34. J. H. Sinfelt, *Acc. Chem. Res.* **1987**, *20*, 134.
35. W. M. H. Sachtler, *Cat. Rev.-Sci. Eng.* **1976**, *14*, 417.
36. V. Ponec, W. M. H. Sachtler, in *Proceedings 5th International Congress on Catalysis*, 1972, North-Holland Publishers, Amsterdam, 1973, pp. 6541–6557.
38. H. Verbeek, W. M. H. Sachtler, *J. Catal.* **1976**, *42*, 257.
39. W. M. H. Sachtler, *Le Vide* **1973**, *163–165*, 9.
40. F. Stoop, F. J. C. M. Toolenaar, V. Ponec, *J. Chem. Commun.* **1981**, 1024.
41. F. J. C. M. Tolenaar, V. Ponec, *J. Catal.* **1983**, *83*, 253.
42. W. M. H. Sachtler, G. J. H. Dorgelo, *J. Catal.* **1965**, *4*, 654.
43. W. M. H. Sachtler, R. Jongepier, *J. Catal.* **1965**, *4*, 665.
44. W. M. H. Sachtler, R. A. van Santen, *Appl. Surf. Sci.* **1979**, *3*, 121.
45. W. M. H. Sachtler, *Appl. Surf. Sci.* **1984**, *19*, 16.
46. M. A. Newton, S. M. Francis, Y. Li, D. Law, M. Bowker, *Surf. Sci.* **1991**, *259*, 45.
47. A. Schoeb, T. J. Raeker, L. Yang. X. Wu, T. S. King, A. E. DePristo, *Surf. Sci. Lett.* **1992**, *278*, L125.
48. N. T. Andersen, F. Topsøe, I. Alstrup, J. R. Rostrop-Nielsen, *J. Catal.* **1987**, *104*, 454.
49. J. A. Oliver, C. Kemball, *Proc. Roy. Soc. (London)* **1990**, *A-429*, 17.
50. J. H. Sinfelt, *J. Catal.* **1973**, *29*, 308.
51. J. H. Sinfelt, *Bimetallic Catalysts*, Wiley, New York, 1983.
52. M. W. Smale, T. S. King, *J. Catal.* **1989**, *119*, 441.
53. M. W. Smale, T. S. King, *J. Catal.* **1990**, *120*, 335.
54. F. M. Dautzenberg, J. N. Helle, P. Biloen, W. M. H. Sachtler, *J. Catal.* **1980**, *63*, 119.
55. H. Verbeek, W. M. H. Sachtler, *J. Catal.* **1976**, *42*, 257.
56. P. Sabatier, *Catalysis in Organic Chemistry*, D. van Nostrand Co., New York, 1925.
57. A. A. Balandin, in *Advances in Catalysis and Related Subjects*, D. D. Eley, H. Pines, P. B. Weisz (Eds.), Academic Press, New York, 1958, Vol. 10, pp. 96–130.
58. A. A. Balandin, *Z. physik. Chemie (Leipzig)* **1929**, *B3*, 167.
59. J. Fahrenfort, L. L. van Reijen, W. M. H. Sachtler, in *The Mechanism of Heterogeneous Catalysis*, J. H. de Boer, et al. (Eds.), Elsevier, Amsterdam, 1960, pp. 23–48.
60. W. M. H. Sachtler, J. F. Fahrenfort, *Proceedings 2nd International Congress of Catalysis, 1960*, Editions Technip, Paris, 1961, pp. 831–863.
61. G. Ertl, *Adv. Catal.* **1990**, *37*, 213.
62. V. Gorodetskii, W. Drachsel, J. H. Block, *Catal. Lett.* **1993**, *19*, 223.
63. M. F. H. van Tol, J. de Maaier-Gielbert, B. E. Nieuwenhuys, *Chem. Phys. Lett.* **1993**, *205*, 207.
64. I. H. B. Haining, C. Kemball, D. A. Whan, *J. Chem. Res.* **1978**, *364*, 2056.
65. G. Leclerq, H. Charcosset, R. Maurel, C. Bétizeau, C. Bolivar, R. Frety, D. Jaunay, H. Mendez, L. Tournayan, *Bull. Soc. Chim. Belg.* **1979**, *88*, 577.
66. S. N. Augustine, W. M. H. Sachtler, *J. Phys. Chem.* **1987**, *91*, 5935.
67. M. J. P. Botman, K. de Vreugd, H. W. Zandbergen, R. de Block, V. Ponec, *J. Catal.* **1989**, *116*, 467.
68. F. H. Ribeiro, A. L. Bonivardi, G. A. Somorjai, *Catal. Lett.* **1994**, *27*, 1.
69. Y. L. Lam, J. Criado, M. Boudart, *Nouveau J. Chimie* **1977**, *1*, 461.
70. V. K. Shum, J. B. Butt, W. M. H. Sachtler, *J. Catal.* **1985**, *96*, 371.
71. S. M. Augustine, G. N. Alameddin, W. M. H. Sachtler, *J. Catal.* **1989**, *115*, 217.

5.3.4
Promoters and Poisons

Bruce E. Koel and Johoo Kim*

5.3.4.1 Introduction

Catalysts are modified by promoters and poisons, which are substances added deliberately or present accidentally, that affect the activity, selectivity, and lifetime of the catalyst. Modifications of these properties have been of interest since catalysts were discovered and further developed for commercial use. The equivalent chapter in the First Edition of this Handbook provided a brief review and perspective of this early history. The action of these modifiers has enormous consequences for catalyst performance. For example, without potassium as a promoter, the iron-based ammonia synthesis catalyst developed during the 1910s would not be practical, while the poisoning effects of lead on the three-way (Pt, Pd, Rh) automotive exhaust catalysts forced the elimination of tetraethyl lead as an additive in gasoline during the late 1970s. The current emphasis on developing catalysts that are ever more selective forces attention to be focused on improving our understanding of the mechanism of action of promoters and poisons.

With regard to the scope of this chapter, it should be noted that there are three major types of catalyst: (i) electronic (oxidation-reduction, metals); (ii) acidic (ionic compounds); and (iii) structural (molecular sieves, zeolites). In each of these types, the chemical composition, structure, and preparation methods all affect catalyst properties, albeit in different ways. Similarly, the action of promoters and poisons is different in each catalyst type (although limitations of space prevent a complete discussion of these effects here). Neither will many interesting and timely topics, such as photocatalysis and electrocatalysis, be discussed specifically at this point. However, a brief overview and context for discussion of promotion and poisoning in each of five classical reactions is provided. These reactions were selected in part because of the detailed, molecular-level studies that are now available, and whilst the recent literature is cited the interested reader is also referred to other, earlier reviews. In addition, a detailed discussion of four case studies of reactions is provided as excellent examples of modifier action, together with current research using modern spectroscopic methods and a surface science approach. The reader should also note the impact that theory and simulation is currently having on our understanding of these systems.

References see page 1620
* Corresponding author.

5.3.4.2 Modifiers in Catalysis

Three important characteristics of catalysts are:

- activity – the specific rate of reaction in numbers of product molecules per site per second
- selectivity – the propensity for one reaction channel out of many feasible channels
- lifetime – the time of useful catalyst performance.

Modifiers, which usually are present in minor concentrations compared to the bulk of the catalyst material, can affect any or all of these characteristics simultaneously. These modifiers may be present in the catalyst as impurities, or they may accumulate from the reactant stream. In this way they may act to affect the physical structure or electronic structure of the catalyst, or function separately as a catalyst in their own right in a bifunctional mechanism. For supported metal heterogeneous catalysts, modifiers can affect the support or the metal particles. This can occur at even trace amounts, because it is often the case that only a small percentage of surface atoms of the catalyst do all the work, and thus only a small amount of modifier is needed to affect these critical sites.

It has been said, ''One man's promoter is another man's poison''. This is true, since a *promoter* is a modifier that has desirable, beneficial effects on catalyst performance. A *poison* is a modifier that has undesirable, detrimental effects on catalyst performance. Of course, whether a given chemical or additive acts as a promoter or a poison depends not only on the type of catalyst, but also on the type of reaction over a given catalyst. For example, potassium is a promoter for Fe-catalyzed ammonia synthesis and a poison for Pt-catalyzed hydrogenations. Ultimately, the electronic structure of the catalytic site controls the bonding of reactants, intermediates, and products of the reaction, and thus activation energy barriers in elementary steps associated with catalytic conversion. Modifiers can affect the number and types of reactive site presented at the catalyst surface, or they can affect the subtle chemical nature of a given reactive site.

5.3.4.2.1 **Structural Modifiers** Additives that restructure the catalyst surface, changing surface area, affecting pore size and distribution, influencing the size, shape, and crystalline nature of nanoparticles or phases, affecting the dispersion of metal components by enhancing or inhibiting sintering or migration, or changing the crystal facets exposed for reaction, are called ''structural modifiers''. Such beneficial additives are also called ''textural promoters''.

5.3.4.2.2 **Bonding Modifiers** Sulfur often functions as a poison (e.g., in Ni catalysts for CO hydrogenation) because it strongly bonds to chemically reactive or important sites on metals, blocking sites where it is bonded and/or changing the electronic structure at adjacent sites due to charge transfer or rehybridization of the metal valence band orbitals. Such additives, which are called ''bonding modifiers'', change the adsorption energies of reactants, products, and intermediates, and alter activation energies for forming reaction intermediates. The action of these modifiers can sometimes be interpreted in terms of their relative electronegativities. Halogens and alkali metals often are strong bonding modifiers.

A special case exists in alloy catalysts, in which two or more metal components are intimately mixed to form mixed ensembles of reactive sites at the alloy surface. Historically, discussions of the influence of one metal on another have centered on electronic (ligand) effects or geometric (ensemble, site-blocking) effects. In addition, each metal of the mixed ensembles may also play a direct role rather than simply modifying the properties of the other. The recognition of the importance of surface segregation, in which the concentration of one component can be strongly enhanced in the surface layer compared to its bulk concentration, and the revelation that reactive sites are at most a few atoms in size, have blurred these distinctions in recent times, and today a better focus is one of ''site-directed'' chemistry in which the composition and structure of a four- or five-atom ensemble is specified and structure–reactivity relationships are established.

Below, several cases are considered which involve catalytic reactions over specific catalysts modified by a particular additive in which the fundamental basis for the role of the modifier has been explored in detail. These include characterization of the performance and structure of the practical, working catalyst and model studies utilizing surface science experiments and theoretical calculations on well-defined surfaces. In these cases, there appears to be a good understanding of the specific mechanism of action and origin of the influence of the modifier.

5.3.4.3 Promoters and Poisons for Some Important Catalytic Reactions

5.3.4.3.1 **Steam Reforming** Steam reforming of coke and natural gas is an important process used to produce hydrogen and synthesis gas (syngas; $CO + H_2$). Recently, energy concerns have led to an increased interest in hydrogen as an energy source, and syngas is an important intermediate in the industrial synthesis of various chemicals and fuels from a wide variety of feedstocks. Even though steam reforming has been commercialized since the 1960s, using Ni-based catalysts, much recent effort has been invested in improving the efficiency of the process. In these catalysts, Ni particles are

highly dispersed on support materials such as alumina (Al_2O_3), magnesia (MgO) or magnesium aluminum spinels ($MgAl_2O_3$) [1]. The reactions involved in the steam reforming of natural gas can be summarized as follows:

$$CH_4 + H_2O \longrightarrow CO + 3H_2$$
$$\Delta H^0_{298} = +206\,\text{kJ mol}^{-1} \quad (1)$$
$$CO + H_2O \longrightarrow CO_2 + H_2$$
$$\Delta H^0_{298} = -41\,\text{kJ mol}^{-1} \quad (2)$$
$$C_nH_{2n+2} + nH_2O \longrightarrow nCO + (2n+1)\,H_2$$
$$\Delta H^0_{298} > 0 \quad (3)$$

Since the reaction in Eq. (1) is endothermic and the entropy is positive, it is better to carry out the reaction at high temperature (900–1300 K) and low pressure (20–40 bar; $20–40 \times 10^5$ Pa). Catalysts for steam reforming must be robust to remain active for a long time under these severe conditions. In this section, some recent studies of additives on Ni catalysts will be reviewed, with special focus on their promoting and poisoning effects.

A Reactive Sites on Ni Catalysts While the nature of the active sites on these Ni catalysts remains the subject of much debate, theoretical and experimental results have suggested that step sites are the main active sites [2–5]. Methane decomposition on Ni single crystals indicates that the Ni(110) surface is the most reactive, followed by Ni(100), with Ni(111) being the least active [6]. Density functional theory (DFT) calculations for methane and ethylene dissociation on Ni(111) and Ni(211) surfaces indicate that step sites are more reactive than terrace sites due to a lower activation energy for dissociation on step sites [2, 5]. Figure 1 shows a potential energy diagram for C–C and C–H bond breaking in ethylene adsorbed on Ni(111) and Ni(211) [5]. The adsorption energy of ethylene on Ni(211) is lower than on Ni(111) by 58 kJ mol^{-1}, and the transition state energy for C–C bond breaking of ethylene on Ni(211) is lowered by 96 kJ mol^{-1}, which in turn lowers the activation energy of ethylene dissociation by 38 kJ mol^{-1}. Scanning tunneling microscopy (STM) images of ethylene exposed on Ni(111) at room temperature (see Fig. 2) show that ethylene dissociation occurs at the upper step edges and terminates once it extends up to 40 Å into the terrace. In experiments where methane ($p = 0.1 - 10^2$ Pa) was exposed to a Ni(14 13 13) surface, which has a step density of 3–5%, at 500 K [3], the initial sticking probability on step sites was two orders of magnitude greater than that on terrace sites. Carbon produced from methane decomposition also indicated that methane is decomposed more rapidly on step sites than on terrace sites.

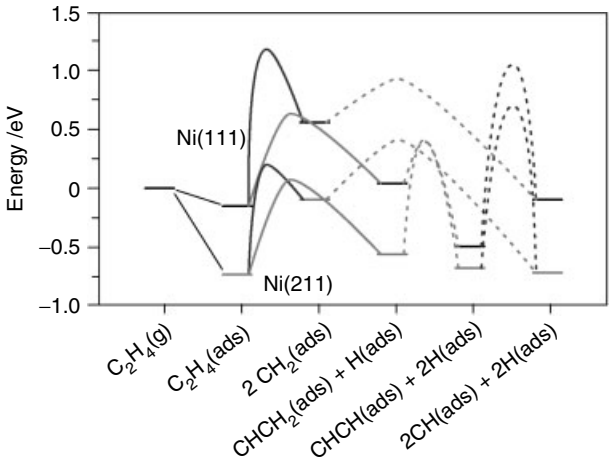

Fig. 1 Potential energy diagram for C–C bond breaking (dark lines) and C–H bond breaking (gray lines) on Ni(111) and Ni(211). The indicated transition state energy for C–H bond breaking of CH_2 is for one CH_2 [5].

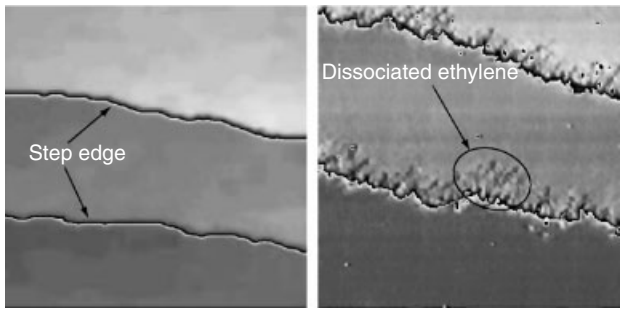

Fig. 2 Scanning tunneling microscopy (STM) images (200 × 200 Å and 150 × 150 Å) of a Ni(111) surface (a) before and (b) after exposure to 1-Langmuir ethylene at room temperature. Exposure produces a "brim" of reaction products adsorbed along the step edges. A cyclic scaling has been used to enhance the features of each terrace [5].

B Alkali and Alkaline Earth Promoters for Ni Catalysts Alkali and alkaline earth metals are added to Ni catalysts to improve stability and selectivity. These additives help to increase the steam–carbon reaction and suppress cracking and polymerization by neutralizing the acidity of the support. The effects of these additives are dependent on the properties of the support. Chen et al. [7] investigated additive effects on the resistance to coke formation and sintering on Ni/Al_2O_3 catalysts. The resistance to Ni sintering was improved significantly by adding various promoters (as shown in Table 1), but only K was found to suppress coke formation. Gołębiowski et al. [8] found that the addition of K (in the form of K_2O) to Ni

References see page 1620

catalysts decreased the catalytic activity for methane steam reforming at 600–800 °C, but significantly increased the resistance to coking. Figure 3 shows the relative coking rate in steam reforming of *n*-butane and relative activity in steam reforming of methane on $K/Ni/Al_2O_3$ catalysts. To help understand the role of K promotion, DFT calculations were carried out by Beengaard et al. [9] for dissociative chemisorption of methane on Ni(100) and Ni(111) surfaces with preadsorbed K adatoms. The initial sticking probability of methane was decreased significantly with K addition, and the barrier for methane dissociation was increased by 0.2 eV on both surfaces with $\theta_K = 0.125$ monolayer. These authors later proposed that K adsorbs preferentially on highly undercoordinated sites at Ni surfaces, which leads to a higher tolerance towards graphite formation on Ni catalysts [2].

Tab. 1 Alkali and alkaline earth metal effects on the particles sizes of NiO and Ni for Ni/Al_2O_3 catalysts for (i) calcined, (ii) calcined and reduced, and (iii) used catalyst samples. Used catalyst samples were obtained after catalytic cracking of *n*-hexane for 5 h [7]

	Ni particle size/Å			
Catalyst-additive	*NiO (calcined)*	*Fresh*	*Used*	*Ratio (used/fresh)*
Ni	131	161	259	1.6
Ni–Li	142	226	298	1.3
Ni–Na	139	158	231	1.4
Ni–K	157	206	214	1.0
Ni–Mg	167	227	258	1.1
Ni–Ca	198	241	283	1.1

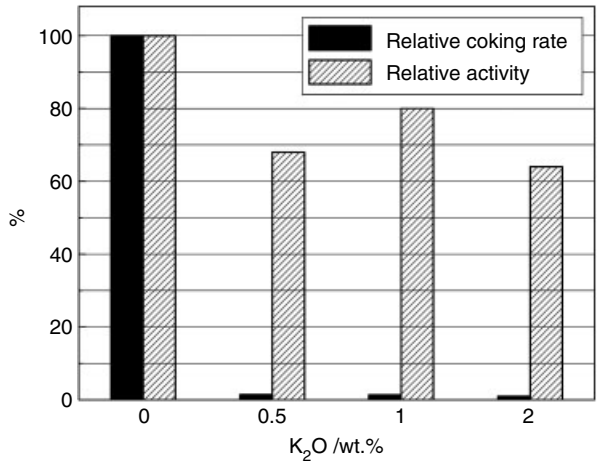

Fig. 3 Relative coking rate (solid) during steam reforming of *n*-butane and relative activity (hatched) during steam reforming of methane on $K/Ni/Al_2O_3$ catalysts. Steam reforming of methane was conducted at 10^5 Pa and 800 °C; steam reforming of *n*-butane was conducted at $p_{butane} = 6.1$ kPa and 500 °C [8].

In investigations of the influence of Li addition to Ni/MgO catalysts [10, 11], Li improved the reducibility of Ni/MgO catalyst by extracting Ni^{2+} from the MgO support. Li also affected the morphology of the catalysts and lead to sintering which reduced the chemisorption ability of the Ni/MgO catalysts.

Methane conversion was increased by 50% for Ni/α-Al_2O_3 catalysts containing 5 wt.% Mg and Ca with respect to unpromoted catalysts [12]. Temperature-programmed reaction spectroscopy (TPRS) experiments demonstrated that these promoters enhanced methane steam reforming, without altering the reaction mechanism. Mg addition also promoted steam reforming by assisting the oxidation of formed coke and hosting a higher content of hydrogen on the catalysts.

C Sulfur Poisoning of Ni Catalysts Sulfur is a powerful poison of Ni catalysts, and thus the S content of the feed gas is reduced below 0.5 ppm [13, 14] prior to steam reforming processes, often by using ZnO catalysts for hydrodesulfurization [15]. All sulfur-containing compounds in the feedstock are converted into H_2S under reforming conditions, and H_2S dissociatively adsorbs on the Ni surfaces to create Ni–S species that deactivate the catalyst.

While large amounts of sulfur poisons Ni catalysts, a small amount of S can promote the catalyst by delaying coke formation. Thus, negative effects of S in decreasing catalytic activity are partially offset by inhibiting coke formation, which also decreases catalytic activity. Rostrup-Nielsen [16] reported for Ni catalysts that S blocks the Ni surface sites necessary for nucleating carbon. Kikowatz et al. [17] investigated the effects of S on the decomposition of hydrocarbons on a polycrystalline Ni film at high temperatures. In these studies, hydrocarbon decomposition eventually produced a monolayer of surface graphitic carbon that deactivated Ni for further hydrocarbon decomposition. Figure 4, which shows the amount of carbon formation on the Ni surface with and without H_2S in the reactant gas mixture, clearly demonstrates that sulfur delays the formation of the carbon monolayer.

The effect of S adatoms on the dissociative adsorption of lower alkanes also has been examined on Ni(100) surfaces [18, 19]. Figure 5 shows the initial rate of methane decomposition at a methane partial pressure of 130 Pa on Ni(100) at 550 and 600 K as a function of S coverage. The reaction rate decreased as the amount of sulfur increased. An Arrhenius activation energy for methane dissociative adsorption on the sulfur covered surfaces was determined to be 27 kJ mol^{-1}, which is similar to that from clean Ni(100) [6]. This suggests that sulfur atoms are simply blocking sites without

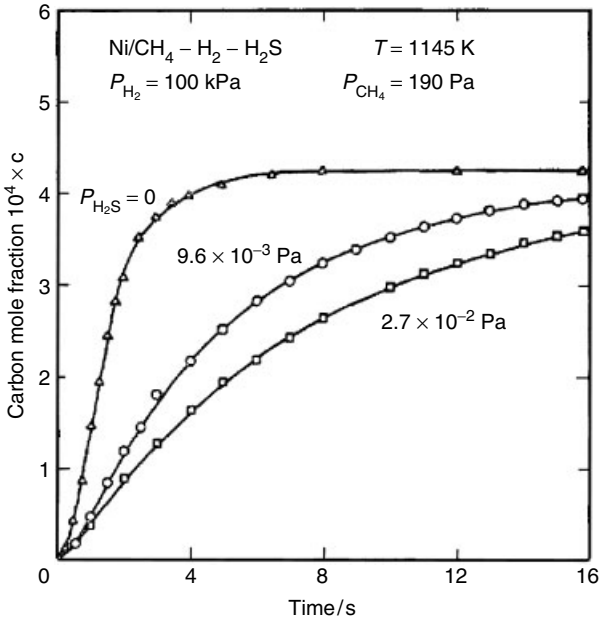

Fig. 4 Carbon mole fraction x_C as a function of reaction time on a polycrystalline Ni film at 1145 K exposed to a gas mixture of $CH_4/H_2/H_2S$. The partial pressures of H_2 and CH_4 were constant at 100 and 190 Pa, respectively. The partial pressure of H_2S was 9.6×10^{-3} Pa and 2.7×10^{-2} Pa, as indicated [17].

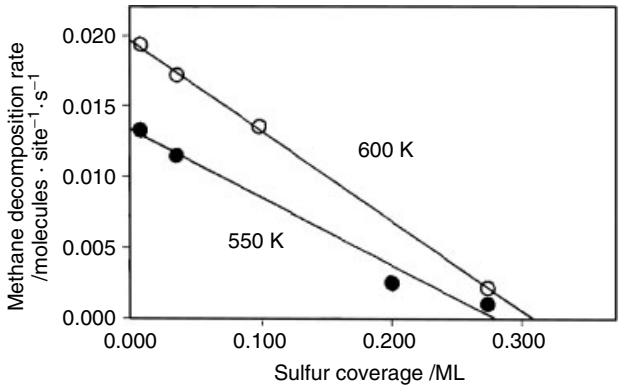

Fig. 5 The initial decomposition rate of methane exposed on a Ni(100) surface at 550 and 600 K as a function of the sulfur precoverage. The partial pressure of methane was 130 Pa [18].

changing the reaction mechanism, and this agrees well with previous results on Ni catalysts [16]. Consistently, Abild-Pedersen et al. [3], in investigations of the influence of S on methane decomposition on the stepped Ni(14 13 13) surface at 500 K, found that a small amount of sulfur (0.06 monolayer) reduced the initial sticking probability of methane and significantly delayed coke formation on the surface.

DFT calculations of S adsorption and the influence of S on carbon formation on Ni(111) and Ni(211) surfaces [2, 3] found that S adsorption at step sites was favored by 37 kJ mol^{-1} with respect to terrace sites. Because carbon nucleation is only initiated at step edges [5], the strong preference of S for steps would greatly hinder carbon formation on Ni surfaces.

5.3.4.3.2 **Water-Gas Shift Reaction** The water-gas shift (WGS) reaction is one of the most important industrial reactions. It is used to produce hydrogen for ammonia synthesis, is a part of steam reforming and automotive exhaust gas catalysis, and is employed for removing CO from H_2 feeds and adjusting the ratio of H_2 and CO in syngas. WGS reactions occur whenever CO and water coexist during catalytic processes. This reaction, shown earlier in Eq. (2), is moderately exothermic at room temperature with no change in entropy.

Although many metals and metal oxides have been tested as WGS catalysts [20, 21], Fe_3O_4/Cr_2O_3 and $Cu/ZnO/Al_2O_3$ are currently employed industrially. Fe_3O_4/Cr_2O_3 catalysts are used in a first stage at 300–450 °C, while $Cu/ZnO/Al_2O_3$ catalysts are in a second stage at 150–250 °C to ensure completion of the reaction. The apparent activation energy for CO conversion to CO_2 was determined to be 53 kJ mol^{-1} for $Cu/ZnO/Al_2O_3$, and 110 kJ mol^{-1} for Fe_3O_4/Cr_2O_3 [22].

Two types of WGS reaction mechanism have been proposed: an adsorptive mechanism, and a regenerative mechanism [23, 24]. In the former, both reactants adsorb on the catalyst surface and react to form surface-bound formate ($HCOO^-$) intermediates. These species then decompose to produce CO_2 and H_2 [25]. In the regenerative mechanism, CO and H_2O adsorb onto the surface and H_2O(a) decomposes into 2H(a) + O(a). Some CO(a) also decomposes to C(a) + O(a). CO(a) reacts with O(a) to form CO_2 and 2H(a) desorbs slowly as H_2 [26]. In addition, a mechanism with both adsorptive and regenerative reaction steps has been suggested [27]. In this case, H_2O adsorbs rapidly and reacts with O(a) to form 2OH(a). 2OH(a) decomposes slowly to 2O(a) and $2H_2$. CO reacts with O(a) to slowly form CO_2(a) that desorbs later. Recent theoretical calculations for the WGS reaction on a Cu(111) surface suggests that the adsorptive reaction path is dominant at lower temperatures, while the regenerative path prevails at higher temperatures [28].

A Iron-Based Catalysts: High-Temperature Shift Catalysts

a Structural Modifiers in Iron-Based Catalysts The active phase of iron oxide for WGS reactions is Fe_3O_4 (magnetite), which is formed by the partial reduction

References see page 1620

of Fe_2O_3 (hematite). A pure magnetite catalyst loses catalytic activity quickly due to sintering during catalytic reaction at 300–400 °C. Therefore, 5–10 wt.% chromia (Cr_2O_3) is added in the industrial catalyst as a structural stabilizer [29]. Several studies have proposed mechanisms of action for chromia in catalyst stabilization. Chinchin et al. [30–32], in investigations of the activity of various Fe_3O_4/Cr_2O_3 catalysts, showed that deactivation was a multistep process in which the first step of rapid deactivation occurred during the first 150 h, and the second step of slow deactivation occurred over several years. These authors found that the catalyst lost 30% of its catalytic activity over the first 9 months, and that the mean pore size increased over the same period, indicating that sintering was the main cause of deactivation. The first rapid deactivation came from the sintering of Fe_3O_4 crystallites in contact, while the second slow deactivation process was due to intervening chromia crystallites separating Fe_3O_4 crystallites and retarding sintering. Recently, Edward et al. [33] found that chromia formed a solid solution within the Fe_3O_4 lattice without forming isolated phases in their investigations of the effect of chromia on magnetite. Chromia encapsulated catalyst grains and reduced ion diffusion, which lead to a retardation of sintering in the activated catalysts.

Other metal oxides have been investigated as structural modifiers. Rethwisch and Dumesic [34] studied SiO_2, Al_2O_3, TiO_2, MgO, ZnO, and Na-mordenite, and found that the activities of all supported iron catalysts were considerably lower than that of pure Fe_3O_4. These authors attributed the reduced activity to the increased acidity that restrains CO adsorption on catalysts with added acidic oxides. On basic oxides, strong CO_2 adsorption hinders the WGS reaction. De Souza and Rangel [35, 36] compared an Al_2O_3 modifier with Cr_2O_3-doped Fe_3O_4. Even though the alumina-doped catalyst showed a slightly smaller catalytic activity than the chromia-doped catalyst, alumina was more efficient in delaying sintering of the catalyst than chromia. Vanadium was reported to be a promising additive for promoting the activity and stability of iron catalysts, and Júnior et al. [37] tested various amounts of vanadium-doped iron oxide catalysts for WGS reactions. Vanadium oxide additives not only increased the specific surface area but also hindered sintering. Vanadium-doped iron oxide catalysts also showed larger catalytic activities than unpromoted and chromia-promoted iron oxide catalysts.

b Metal and Metal Oxides as Promoters for Catalytic Activity

Several metals and metal oxides have been probed as promoters in the iron-based catalysts. For example, Andreev and coworkers [21, 38] investigated the effects of metal oxides on iron oxide catalysts. The catalytic activity for WGS decreased when MnO, CoO, CuO or ZnO were added to pure iron oxide. However, adding CuO, CoO and ZnO (5 wt.%) to iron/chromia catalysts slightly increased the catalytic activity. Unfortunately, the CuO-promoted catalyst exhibited higher sintering than the unpromoted iron/chromia catalysts.

Hutchings and coworkers [39] investigated iron-based catalysts containing 2 wt.% of B, Cu, Ag, Ba, Hg, and Pb. The efficiencies and activation energies for CO conversion over Fe_3O_4/Cr_2O_3 catalysts containing these additives are listed in Table 2. Catalytic activity was increased by all additives except boron, with the order of activity found as be Hg > Ag, Ba > Cu > Pb > unpromoted, B. Despite the fact that boron did not increase the activity, it did decrease the activation energy for CO conversion along with other additives. The promoting activities of Hg, Ag and Ba were attributed to changes in the electronic nature of the catalyst influenced by the different ionic sizes of these additives.

The role of copper has also been examined in detail, by Hutchings and coworkers [33, 40]. The activation energy for WGS over $CuO/Fe_3O_4/Cr_2O_3$ catalysts was estimated as 75–80 kJ mol^{-1}, while that on Fe_3O_4/Cr_2O_3 catalysts was 118 ± 9 kJ mol^{-1}. Structural studies of the Cu-promoted catalyst demonstrated that CuO and Cr_2O_3 were in solid solutions within the Fe_3O_4 phase in the fresh catalyst, as shown in Fig. 6. Cr and Cu were enriched at the surface of iron oxide crystallites in aged catalysts. High-resolution electron microscopy (HREM) images also showed CuO to be segregated from the Fe_3O_4 phase on the surface of 1000-h aged CuO-doped catalysts, indicating sintering of the catalyst.

Rhodium has shown good promoting effects on the catalytic activity on Fe_3O_4/Cr_2O_3 catalysts [41–43]. Figure 7 shows WGS rates over Fe_3O_4/Cr_2O_3 catalysts that have been doped with precious metals [42]. Rh-promoted Fe_3O_4/Cr_2O_3 catalysts exhibited significantly

Tab. 2 Efficiency and activation energy for CO conversion over Fe_3O_4/Cr_2O_3 catalysts containing additives. The reactions were conducted at 400 °C and 28×10^5 Pa. Activation energy values have uncertainties of ±4 kJ mol^{-1} [39]

Additive	*CO conversion/%*	*Activation energy/kJ mol^{-1}*
None	18.8	112
B	18.7	108
Pb	25.0	90
Cu	27.9	81
Ag	32.9	74
Ba	33.5	83
Hg	37.4	82

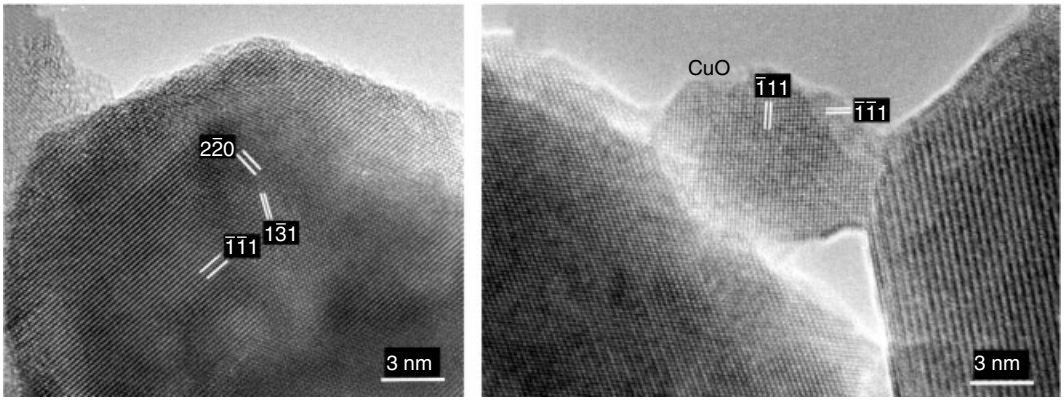

Fig. 6 High-resolution electron microscopy (HREM) images of (a) fresh and (b) 1000-h aged $CuO/Fe_3O_4/Cr_2O_3$ catalysts. In the aged catalyst, CuO segregated from Fe_3O_4 crystallites [33].

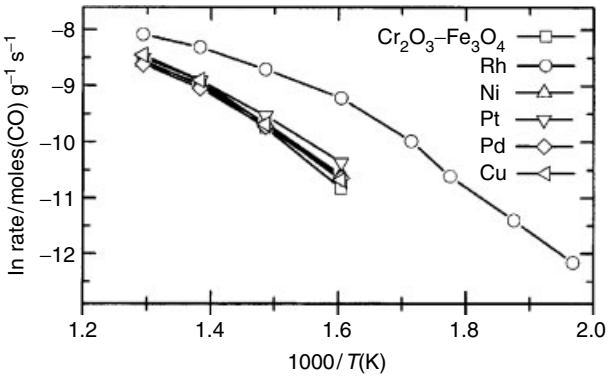

Fig. 7 Arrhenius plots for the water-gas shift reaction over transition metal-promoted Fe_3O_4/Cr_2O_3 catalysts [42]. The Rh-promoted catalyst showed the highest reaction rate.

improved activity. From investigations of the adsorption of each reactant and product on the catalyst, it was determined that the Rh promoter greatly effected the reactivity of CO and hydrogen.

B Copper-Based Catalysts: Low-Temperature Shift Catalysts

a Structural Modifiers In order to explore the most active phase of copper in WGS reactions, Wang and coworkers [44–46] performed DFT calculations using the unity-quadratic exponential potential (UBI-QEP) on reactants and products in WGS on Cu(111), Cu(100) and Cu(100) surfaces. Values for the activation energy of H_2O dissociation, a rate-determining step in the WGS reaction, were in the order: Cu(110) < Cu(100) < Cu(111). Calculated values agreed well with experimental values [25, 47], showing that Cu(110) was the most active and Cu(111) was the least active in H_2O dissociation.

Activity and structure sensitivity of the WGS reaction on Cu/Zn/Al mixed-oxide catalysts were investigated by Ginés et al. [48]. $Cu/ZnO/Al_2O_3$ catalysts showed significantly higher catalytic activity than Cu/ZnO catalysts. The turnover frequency (TOF) for WGS of the samples tested was nearly the same, regardless of the changing surface area and dispersion of copper, which indicates that WGS is a structure-insensitive reaction over these catalysts. The specific reaction rate was proportional to the Cu surface area. The effect of calcination temperature on Cu/ZnO-based catalysts was tested by Saito et al. [49], who found the surface area of the catalysts to decrease as the calcination temperature increased. Figure 8 shows CO conversion over $Cu/ZnO/Al_2O_3$ and $Cu/ZnO/ZrO_2/Al_2O_3$ catalysts and the Cu surface area of the catalysts after reaction. The activity of both catalysts follows the trend of Cu surface area decay that occurs at increasing calcination temperatures. However, the activity of $Cu/ZnO/ZrO_2/Al_2O_3$ catalysts was less affected by high-temperature calcinations, indicating that ZrO_2 provides some stability. SiO_2 was added to the $Cu/ZnO/ZrO_2/Al_2O_3$ catalyst to improve catalytic stability [50]. The reaction rate over a 0.8 wt.% SiO_2-promoted catalyst did not change during the initial 500 h on-stream, while the rate on a related unpromoted catalyst dropped by 15% over the same period. It was suggested that the SiO_2 additive prevented crystallization of Cu and ZnO in the catalyst and maintained the surface area of Cu and the catalyst.

b Cesium Modifiers Investigations of the influence of Cs on Cu single crystals used as model catalysts for the WGS reaction [47, 51–53] found that the activity of the

References see page 1620

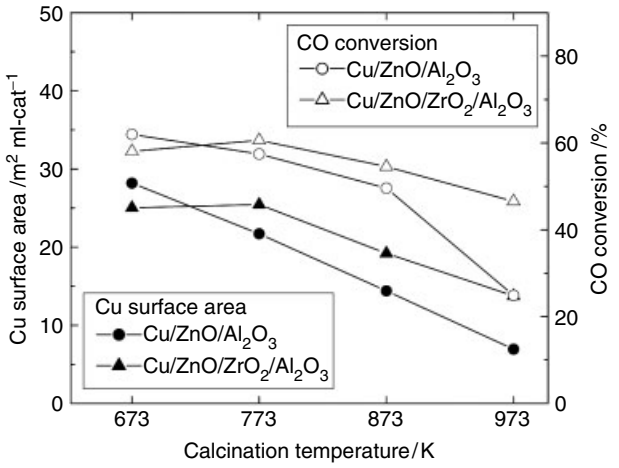

Fig. 8 CO conversion (right axis) and Cu surface area (left axis) after reaction over $Cu/ZnO/Al_2O_3$ and $Cu/ZnO/ZrO_2/Al_2O_3$ catalysts [49]. Catalysts were treated in H_2 at 573 K, and reactions were performed at 523 K and 150 kPa.

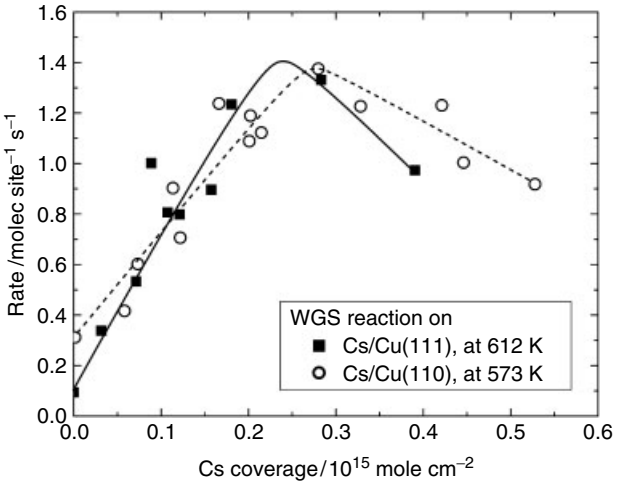

Fig. 9 Water-gas shift (WGS) reaction rate on Cu(111) (■) and Cu(110) (○) surfaces containing cesium. Reactions were conducted at $p_{CO} = 3.5$ kPa and $p_{H_2O} = 1.3$ kPa. This plot was produced from data gathered from Refs. [51] and [47], but a direct comparison of reaction rates is complicated by the different reaction conditions.

Cu(111) surface increased with increasing Cs coverage until $\theta_{Cs} = 2.3 \times 10^{14}$ cm^{-2}, where the rate started to decrease, as shown in Fig. 9. On Cu(110), the maximum rate was obtained at $\theta_{Cs} = 2.7 \times 10^{14}$ cm^{-2}. At maximum enhancement, Cs improved the reaction rate 15-fold on the Cu(111) surface and fivefold on the Cu(110) surface. The apparent activation energy for WGS on Cs-doped Cu(111) of 84 kJ mol^{-1} was close to the value of 71 kJ mol^{-1} for clean Cu(111). Similarly, this value was 46 kJ mol^{-1} for Cs/Cu(110) and 42 kJ mol^{-1} for clean Cu(110), showing that Cs does not reduce the activation energy of the WGS reaction. Adsorption studies of CO, CO_2 and H_2O on the Cs/Cu(110) surface showed that Cs greatly increases the heat of adsorption of H_2O and generates OH(a) even at 110 K [52, 54].

c Sulfur Poisoning Copper-based catalysts are known to be easily poisoned by sulfur, while iron-based catalysts are more resilient [55]. A model study of sulfur poisoning on Cu(111) was reported by Campbell and Koel [56] in which H_2S was adsorbed on Cu(111) at 120 K and dissociated at 200 K to produce S atoms with a maximum coverage of $\theta_S = 0.43$. The WGS reaction was performed over these sulfur-doped Cu(111) surfaces, and it was found that the WGS rate decreased linearly with S coverage. This poisoning effect was attributed to simple blocking of the reaction sites that are needed for H_2O dissociation. Gaseous S_2 was also investigated on polycrystalline Cu, Cu_2O, and Cu/ZnO surfaces [57]. S_2 interacted with metal centers on all of these surfaces with an affinity in the order: Cu > Cu/ZnO > Cu_2O > ZnO. The electron density of Cu decreases when it is bonded to oxygen in ZnO and Cu_2O, making it more difficult to donate electron density to S_2 and break the S−S bond. Therefore, it was proposed that ZnO reduces the activity of Cu toward sulfur and this helps to prevent sulfur poisoning of the Cu catalyst.

5.3.4.3.3 **Methanation** Oxides of carbon (CO and CO_2) are known as poisons for many hydrogenation catalysts, and even small amounts of carbon oxides lead to permanent deactivation of ammonia synthesis catalysts. Thus, methanation of CO and CO_2 is employed in purification of synthesis gases for ammonia and in the production of hydrogen for other uses. Two methanation reactions are:

$$CO + 3H_2 \longrightarrow CH_4 + H_2O \qquad \Delta H^0_{298} = -206.2 \text{ kJ mol}^{-1} \tag{4}$$

$$CO_2 + 4H_2 \longrightarrow CH_4 + 2H_2O \qquad \Delta H^0_{298} = -165.0 \text{ kJ mol}^{-1} \tag{5}$$

Commercial methanation catalysts are based on Ni supported on various oxide mixtures, such as Al_2O_3, SiO_2, CaO, MgO, and $CaAl_2O_4$.

Several models that have been proposed for CO methanation are summarized in Ref. [58]. CO methanation may proceed via formate ($HCOO^-$) intermediates, which have been detected by diffuse reflectance infrared Fourier transform spectroscopy (DRIFTS) [59]. Goodman and coworkers [60] found that CO dissociated under methanation conditions, and that the hydrogenation rate of surface carbon was close to the methanation rate, suggesting carbon hydrogenation as the rate-determining

$$H_2(g) \rightarrow 2H(a)$$
$$CO(g) \rightarrow CO(a) \rightarrow C(a) + O(a)$$
$$C(a) + H(a) \rightarrow CH(a) + H(a) \rightarrow CH_2(a) + H(a) \rightarrow CH_3(a) + H(a) \rightarrow CH_4(g)$$
$$O(a) + H(a) \rightarrow OH(a) + H(a) \rightarrow H_2O(g)$$

Scheme 1

step. Alstrup [58] proposed a mechanism based on the steps below in Scheme 1 in which it was suggested that hydrogenation of CH(a) controls the rate of methanation.

Sehested et al. [61] confirmed CO dissociation at low CO concentration in CO methanation on $Ni/MgAl_2O_4$ catalysts, and proposed CO dissociation to be a rate-determining step, which agreed with a previous report by Mori et al. [62]. The activity of the catalyst increased with CO pressure for low pressures, $p_{CO} < 0.2$ kPa, while it saturated at higher pressures due to diffusion restrictions. The activity increased with increased reaction temperature from 498 to 560 K.

The mechanism of CO_2 methanation is also unclear. There are some experimental reports that CO_2 is converted to CO via the reverse WGS reaction, after which CO hydrogenation proceeds subsequently [59, 63–65]. Schild et al. [66], by using DRIFTS to probe the reaction intermediates of CO_2 methanation on Ni/ZrO_2 catalysts, found that surface carbonates and formates were formed immediately upon CO_2/H_2 flow over the catalyst, while singly and doubly bound CO appeared later. This indicates that formate is an immediate precursor for methane formation. Fujita et al. [59, 63] also detected formates formed on Ni/Al_2O_3 catalysts. These authors observed two types (strongly and weakly bound) of bridge-bonded CO adsorbed on the catalyst, in addition to formates. The strongly adsorbed CO dissociated into C(a) and O(a) and was not affected by H_2. Qin et al. [67] predicted H_2-assisted C−O bond dissociation in CO_2 prior to H_2 dissociation from theoretical calculations of the gas-phase reaction of $H_2/CO_2/Ni$. These authors reported an activation energy of 103.9 kJ mol^{-1} for the reaction: $Ni(^3D) + H_2 + CO_2 \rightarrow Ni(^3D) + H_2O + CO$. The hydrogen migration with water formation was predicted to be the rate-determining step for the overall reaction.

A Active Phase and Structural Modifiers Ni-based catalysts are reported to suffer deep morphological change and to develop ⟨111⟩ planes during the first hours of methanation reactions [68–70]. Results from Ni(111) and Ni(100) surfaces were compared with those on Ni/Al_2O_3 catalysts in the investigations of Goodman and coworkers [71, 72] of CO hydrogenation on Ni single crystal surfaces. Rates of CO hydrogenation were similar, independent of the crystal plane on single crystals or

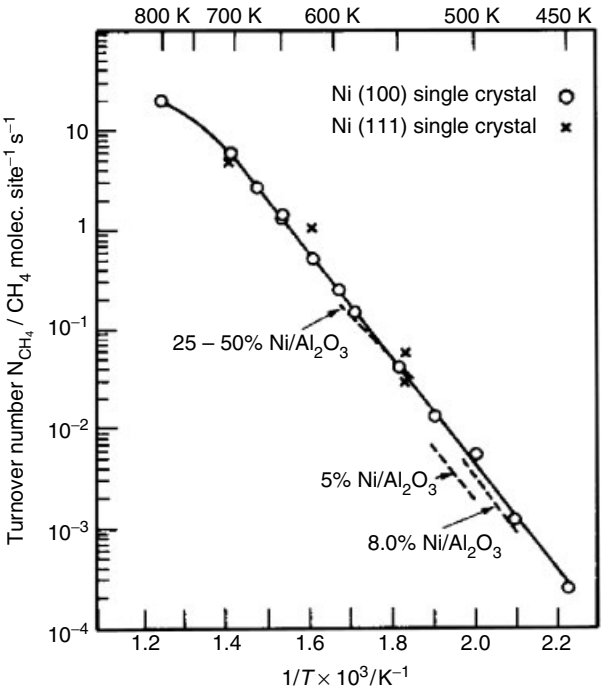

Fig. 10 Arrhenius plot for CO methanation over Ni(100), Ni(100), and Ni/Al_2O_3 catalysts. Reactions were conducted at 16 kPa total pressure with $H_2 : CO = 4 : 1$ [72].

the loading of supported catalysts, as shown in Fig. 10. Agnelli et al. [69] studied CO methanation over Ni/SiO_2 catalysts to obtain information on the reacting surface and aging. These authors found that the working surface of the Ni catalyst did not depend on plane orientation or the presence of specific undercoordinated Ni atoms. The CO hydrogenation rate was related to the probability of hydrogen colliding with CO adsorbed on a Ni atom surrounded by one or two free Ni sites.

The effects of supports (Al_2O_3, SiO_2 and TiO_2) on Ni-based catalysts were investigated by Ozdogan et al. [73] and Bartholomew and Vance [74]. The rate of CO hydrogenation was sensitive to the catalyst support, while the activation energy was not. Reaction rates were in the order: $Ni/TiO_2 > Ni/Al_2O_3 > Ni/SiO_2$. Two sites for methanation were detected on Ni/TiO_2 and Ni/Al_2O_3, but only one for Ni/SiO_2 [73, 75]. The higher activity of TiO_2 as a support was attributed to higher activity for both CO dissociation and carbon hydrogenation [74].

B Electropositive Modifiers Pereira and Martin [70], in their studies of deactivation of alkali-doped Ni/SiO_2 catalysts during CO hydrogenation, found that all catalysts initially experienced deep morphological changes during

References see page 1620

CO hydrogenation. The addition of alkalis stabilized the activity of catalysts by inhibiting Ni sintering. The alkali additives altered the activity for CO hydrogenation on Ni/SiO_2 catalysts in the order: Ni/SiO_2 > $Li-Ni/SiO_2$ > $Na-Ni/SiO_2$ > $K-Ni/SiO_2$. Alkali additives also promoted the formation of carbon deposits that could be easily hydrogenated. Li and Na decreased the selectivity of CO hydrogenation towards CH_4 formation.

The effects of alkali additives (Li, Na, K) on Ni/SiO_2 catalysts were also investigated by Diaz et al. [76], who found Li and K modified the Ni distribution on the silica support resulting in larger Ni particles while Na kept the dispersion of Ni particles. By using DRIFTS, several CO bands on unpromoted, Li- and K-promoted catalysts were observed, while no CO band could be seen on a Na-promoted catalyst, which indicates that CO adsorption was strongly inhibited on the Na-promoted Ni/SiO_2 catalyst.

In studies of CO hydrogenation over Ni(100), Campbell and Goodman [77] found that the addition of potassium decreased the methane formation rate and increased the rate of forming higher hydrocarbons. These authors suggested that this influence of K occurred without changing the reaction mechanism because the K loading did not affect the activation energy.

Falconer and coworkers [78] found that potassium decreased the overall CO hydrogenation activity and the specific activity of methane formation on a Ni/Al_2O_3 catalyst, while it increased the selectivity for production of higher hydrocarbons. K also increased the CO dissociation rate. Figure 11 shows the methane desorption rate from CO hydrogenation over K-promoted Ni(10 wt.%)/Al_2O_3 catalysts. Unpromoted Ni catalysts exhibited two peaks, which indicates two different paths for methane formation. Adding K to the catalyst shifted the desorption peaks to higher temperature, suggesting a higher activation energy and lower activity for the catalyst.

Falconer's group [64] found different results for CO_2 hydrogenation over K-promoted Ni/SiO_2 and $Ni/SiO_2-Al_2O_3$ catalysts, determining that K did not increase the selectivity for higher hydrocarbons, but instead changed the product distribution. Figure 12 shows the methane formation rates on both Ni/SiO_2 and $Ni/SiO_2-Al_2O_3$ catalysts modified by potassium. K addition initially increased the CO and CO_2 hydrogenation rate on $Ni/SiO_2-Al_2O_3$ catalysts, but these rates were then decreased at higher K loadings. In contrast, these rates both decreased on $K/Ni/SiO_2$ catalysts, illustrating that the effects of K promotion depends on the catalyst support.

As a final note, Tavares and coworkers [79, 80] found that a small amount of Cu added to Ni-based catalysts decreased the CO methanation rate, while higher Cu concentrations increased the rate, reaching a maximum at 7 atom% Cu. The rate of carbon formation on the catalyst was increased at small amounts of Cu (1 atom%) and decreased at higher Cu content (no carbon existed at 10 atom% Cu). These results agree with those of Agnelli and Mirodatos [81], who found in addition that the effect of Cu on CO hydrogenation depended on temperature. At low temperatures (503 K), a small amount (3 atom%) of Cu prevented a loss of activity from sintering without considerably diminishing the CO hydrogenation rate. However, at high temperatures (723 K), a large amount (13 atom%) of Cu was needed to reduce surface carbon at the expense of the CO hydrogenation rate.

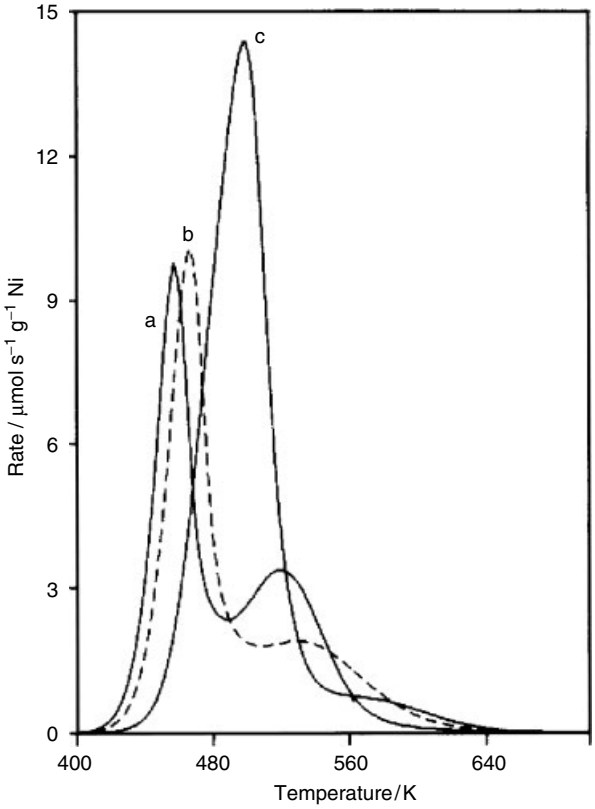

Fig. 11 Methane evolution during temperature programmed reaction of CO adsorbed on K-promoted Ni(10 wt.%)/Al_2O_3 catalysts. K loadings were: (a) 0.02; (b) 0.95; and (c) 3.3 wt.% [78].

C Electronegative Modifiers Considerable attention was paid to the sulfur poisoning of catalysts during the 1970s and 1980s. In summary, sulfur effectively poisons Ni surfaces even at low coverages, and also decreases the sticking coefficient of hydrogen [82, 83]. Rostrup-Nielsen and Petersen [84] showed that sulfur had a non-linear effect on the methanation reaction over nickel catalysts, but did not alter the activation energy. This indicated that sulfur poisoning occurred primarily by a geometric or site-blocking effect. In studies on Ni(100) model catalyst surfaces, Goodman and Kiskinova [85] found a

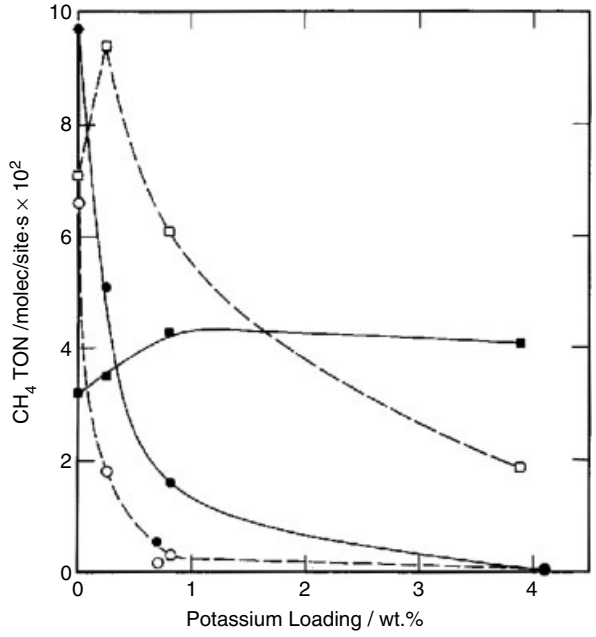

Fig. 12 Methane formation rates as a function of K loading for Ni/SiO_2 (○, ●) and $Ni/SiO_2-Al_2O_3$ (□, ■) catalysts at 553 K. CO_2 hydrogenation is indicated by the solid lines and CO hydrogenation is indicated by the dashed lines [64].

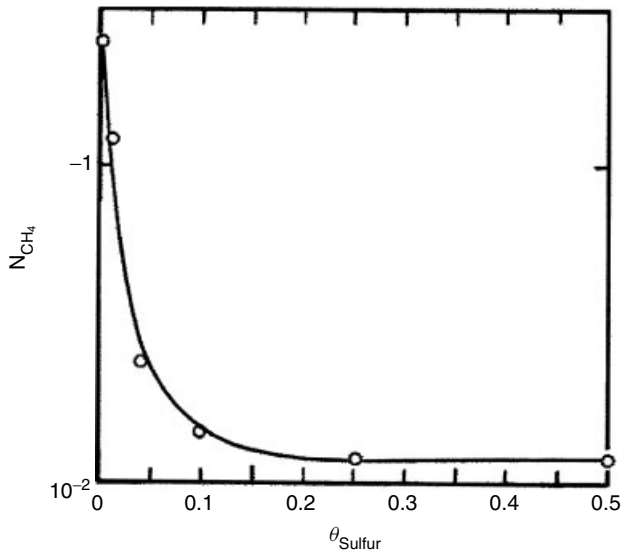

Fig. 13 CO methanation rate as a function of sulfur coverage on a Ni(100) surface. The pressure was 16 kPa, $H_2/CO = 4/1$, and reaction temperature was 600 K [85].

similar effect of sulfur; this non-linear relationship on methane formation is illustrated graphically in Fig. 13. The catalytic activity decreased very quickly at low sulfur coverages ($\theta_S < 0.1$) and reached a maximum deactivation at $\theta_S = 0.25$.

Goodman and Kiskinova [86] also studied the influence of other electronegative atoms, chlorine and phosphorus, on Ni(100) surfaces. Electronegative adatoms reduce the adsorption rate, adsorption energy, and saturation amount of CO and H_2 on Ni(100). These effects increased with increasing electronegativity of the additives, which is in the order Cl > S > P. This variation was attributed to the change in surface electron density caused by the presence of the electronegative adatoms.

5.3.4.3.4 **Fischer–Tropsch Synthesis** Since the invention by Fischer and Tropsch of the conversion of synthesis gas ($CO + H_2$) to aliphatic hydrocarbons [23, 87], the process has been modified to produce a wide range of products. Linear paraffins (alkanes) and α-olefins are often the main products in a mixture of linear, branched and oxygenated hydrocarbons. Reactions for these two products can be written as:

Paraffin formation :

$$(2n+1)H_2 + nCO \longrightarrow C_nH_{2n+2} + nH_2O \qquad (6)$$

Olefin formation :

$$2nH_2 + nCO \longrightarrow C_nH_{2n} + nH_2O \qquad (7)$$

Secondary reactions can occur when primary products desorb and interact with other active sites. Secondary reactions of α-olefins include hydrogenation to n-alkanes, isomerization, cracking, hydrogenolysis, and insertion into growing chains. Fischer–Tropsch (FT) synthesis catalysts are based on Fe, Co, and Ru metals with various promoters. Iron catalysts are commonly used because of their low cost compared to other metals that are active for FT synthesis. Alkali-promoted Fe catalysts have a high activity for WGS reactions and high selectivity for forming olefins. Cobalt catalysts have the advantage of the highest yields, the longest lifetime, and the highest selectivity to form linear alkanes. Although Ru catalysts are very active, they are rarely used due to the high price of Ru.

Mechanisms in FT synthesis have been reviewed extensively [23, 88–92]. The FT synthesis is a polymerization reaction which occurs on the catalyst surface, the most plausible mechanism for the synthesis of linear hydrocarbons being via the carbide mechanism involving CH_2 insertion. First, the reactants CO and H_2 adsorb and dissociate into C(a), O(a) and 2H(a). The adsorbed carbon then reacts with H(a) to initiate a chain reaction and to form methylene groups, CH_2(a). Propagation occurs by CH_2(a) inserting into growing alkyl chains. The chain reaction terminates by abstraction of hydrogen to form an olefin or addition of a hydrogen or methyl group to form a

References see page 1620

paraffin or alkane product. Mechanisms for the synthesis of oxygenated hydrocarbons involve initiation when CO(a) reacts with H_2 or H(a) to form formate species and chain growth by inserting CH_2(a) into formate.

A Fe-Based Catalysts

a Active Phase and Structural Modifiers Several phases of iron have been reported to have catalytic activity for FT synthesis: metallic Fe (α-Fe), iron oxides (α-Fe_2O_3, Fe_3O_4 and Fe_xO), and several forms of iron carbides (ε-Fe_2C, ε'-$Fe_{2.2}C$, Fe_xC, x-$Fe_{2.5}C$ and Fe_3C) [93–102]. The formation and composition of these phases in catalysts depend on the preparation, pretreatment process, and the initial composition of precursors. Overall, carbides are likely to be the key active phases for CO dissociation and hydrogenation, while oxides are active for CO molecular adsorption and for producing oxygenated hydrocarbons.

A major role of the support is to form crystallites of active Fe phases and to prevent sintering. Thus, the support influences not only the stability of the catalyst, but also the activity and selectivity [103, 104]. SiO_2 is the most efficient among supports tested for iron-based catalysts for FT synthesis. Bukur et al. [103] investigated the effects of SiO_2 and Al_2O_3 on the activity and selectivity of iron catalysts (Fe/Cu/K) for FT synthesis. Increasing the amount of these supports decreased the overall catalytic activity. The selectivity for higher α-olefins ($\geq C_9$) was decreased with increasing SiO_2 content, but there was no effect of Al_2O_3 content. The conversion of olefins by isomerization to secondary olefins was increased with increased SiO_2 content. SiO_2 also promoted the production of alcohols, while Al_2O_3 decreased the selectivity for alcohols. Yang et al. [104], for Fe–Mn-based FT catalysts, found that the incorporation of SiO_2 led to a higher surface area and stability. Increasing the amount of SiO_2 reduced the catalytic activity and selectivity to smaller hydrocarbons (C_1–C_4) and olefins. The overall selectivity to oxygenated hydrocarbons decreased with increasing amounts of SiO_2, but the selectivity to alcohols increased.

b Metal Modifiers Iron-based catalysts for FT synthesis are often promoted with alkalis and Cu. As this subject has been extensively reported in the past, only a few recent results will be mentioned at this point. When summarizing past reports (before 1990), alkali additives tend to increase the catalytic activity in the order of K ~ Rb > Na > Li. However, the investigations of Ngantsoue-Hoc et al. [105] showed some of the complexity in these effects. Na-promoted catalysts exhibited the lowest deactivation rates. Figure 14 shows that the K-promoted catalyst had the highest CO conversion and

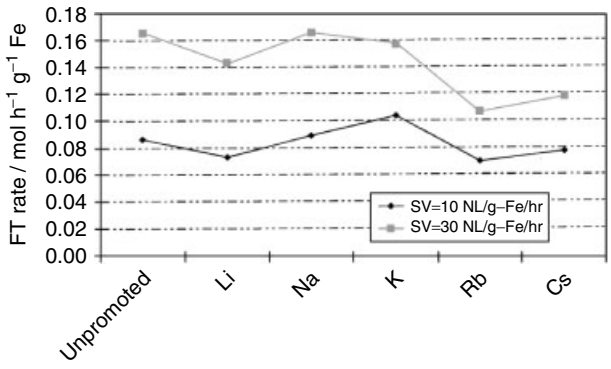

Fig. 14 Fischer–Tropsch (FT) synthesis rates measured for alkali-promoted Fe/SiO_2 catalysts at 543 K. Reactions were performed at 1.3 MPa with $H_2/CO = 0.67$. Potassium addition caused the highest rate at low space-velocity [105].

WGS rate at the lower space-velocity (SV) feed, whereas the Na-promoted catalyst showed the same FT conversion rate as the unpromoted catalyst. Other alkali metals (Li, Cs, and Rb) were less effective in promoting FT synthesis. Cs-, Rb- and K-promoted catalysts showed improved selectivity for unsaturated hydrocarbons.

Bukur et al. [106] found that a small mount of potassium increased the activity for FT synthesis and the WGS reaction over Fe catalysts. Potassium also increased the average molecular weight of hydrocarbon products and suppressed secondary reactions such as the hydrogenation and isomerization of α-olefin products. Figure 15 illustrates this suppression of α-olefin isomerization by small amounts of K at 0–1.0 wt.%. Small

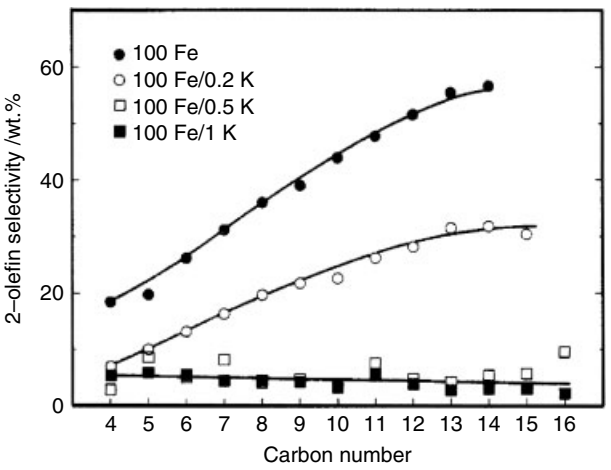

Fig. 15 Selectivity of 2-olefin produced over K-promoted Fe catalysts as a function of carbon number. The 2-olefin selectivity was reduced below 5% by a small amount (0.5–1.0 wt.%) of K. Reactions were conducted at 250 °C and 1.48 MPa with $H_2/CO = 1$ and a flow rate of 2 nL g cat^{-1} h^{-1} [106].

amounts of K inhibited efficiently isomerization reactions from low to high hydrocarbons. K-promoted Fe−Zn catalysts examined by Li et al. [107] had increased rates of CO conversion and Fe_3O_4 carburization. Potassium reduced the selectivity for forming methane and increased the selectivity for producing higher hydrocarbons (C_{5+}) by reducing the concentration of H(a), which terminates the chain reaction. Davis and coworkers [108, 109] found that the effect of potassium in Fe catalysts depended on the CO conversion: the activity decreased with increasing K-loading at lower CO conversion, passed through a maximum at 1.4 atom% K at intermediate conversion, and increased with increased K-loading at higher conversion. The addition of 5 atom% K enhanced the CO conversion rate and increased the selectivity for higher hydrocarbons, but no changes occurred with further K increases.

Luo et al. [110] investigated the effect of alkaline earth metals (Be, Mg, Ca and Ba) on iron-based FT catalysts and compared the results with unpromoted and K-promoted catalysts. The overall FT activities of catalysts with alkaline earth metals were smaller than K-promoted catalysts. Catalysts containing Ba and Mg exhibited CO conversion rates similar to those of unpromoted catalysts, while Be and Ca addition resulted in lower activities than for unpromoted catalysts. Catalysts with alkaline earth metals had less activity for WGS, and Ca and Mg even suppressed the rate of the WGS reaction below that on the unpromoted catalyst. However, the carbon usage rate [i.e., FT rate/(FT rate + CO_2 rate)] was lowest for the K-promoted catalyst and for catalysts with alkaline earth metals. Yang et al. [111] found that Mg addition to $Fe/Cu/K/SiO_2$ catalysts increased the surface area of the catalyst and induced smaller-sized iron crystallites. These authors suggested that an appropriate amount of Mg could improve the activity and stability of the catalyst. Mg increased the selectivity for longer-chain hydrocarbons (C_5-C_{11}), slightly suppressed the WGS reaction, and increased carbon usage.

Cu has been added to iron catalysts to facilitate the reduction of iron oxides during catalyst activation by lowering the reduction temperature with H_2, CO, or syngas [112]. Bukur et al. [106] reported that Cu enhanced the catalyst activity for FT synthesis and WGS. Cu also increased secondary reactions such as olefin hydrogenation and the isomerization of α-olefins. Catalysts containing both Cu and K exhibited higher activity than singly promoted catalysts [106, 113, 114]. On Fe/Zn/K catalysts, Li et al. [107] showed that Cu addition did not affect the surface area, but increased the reduction rate of Fe_2O_3 to Fe_3O_4 under H_2 gas and enhanced the production of methane and paraffins. Cu-promoted $Fe/Mn/K/SiO_2$ catalysts, as shown by Zhang et al. [115], had an increased rate for catalyst activation and a shorter induction period. The product distribution shifted to higher hydrocarbons and olefin formation was enhanced with Cu promotion, as shown in Fig. 16.

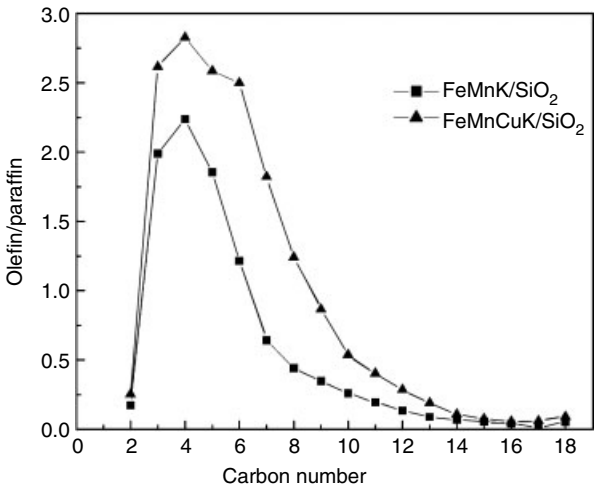

Fig. 16 Olefin/paraffin ratio as a function of carbon numbers in Fischer–Tropsch (FT) synthesis products for promoted Fe/SiO_2 catalysts. The reaction was conducted at 543 K with $H_2/CO = 0.67$ and a CO conversion of 75% [115].

c Sulfur Modification Commonly, sulfur poisons FT catalysts if present even at a low concentration in the syngas feed. However, some studies have shown that sulfur can have promoting effects. For example, Bartholomew and Bowman [116] exposed H_2S to Fe, Fe/SiO_2, $Fe/K/SiO_2$ and Fe/B catalysts at 500 K while monitoring the activity and selectivity with changing sulfur concentration. Surface sulfide formed at low H_2S concentration (<2 ppm) and bulk sulfide formed at higher concentration. The activity decreased with increasing sulfur content in the catalysts except for the Fe/B catalyst, which showed a greater resistance to sulfur poisoning than others. On this catalyst, the activity for CO hydrogenation unexpectedly increased with time for small amounts of H_2S (0.5 ppm); at higher H_2S concentration (8 ppm), only 5% of the activity was lost over several days. In another investigation, Bromfield and Coville [117] added Na_2S in the range of 500 to 20 000 ppm to iron catalysts, and found that catalysts with a low sulfide ion content (500 ppm) exhibited fourfold the FT activity of the pure iron catalyst (see Fig. 17). Sulfide content at 500 to 2000 ppm enhanced the selectivity of olefin formation, but higher loadings (20 000 ppm) poisoned the catalysts. Wu et al. [118] added sulfate (SO_4^{2-}) to $Fe/Cu/K/SiO_2$ catalysts, and found that small amounts of sulfur increased activity and enhanced the selectivity for long-chain hydrocarbons.

References see page 1620

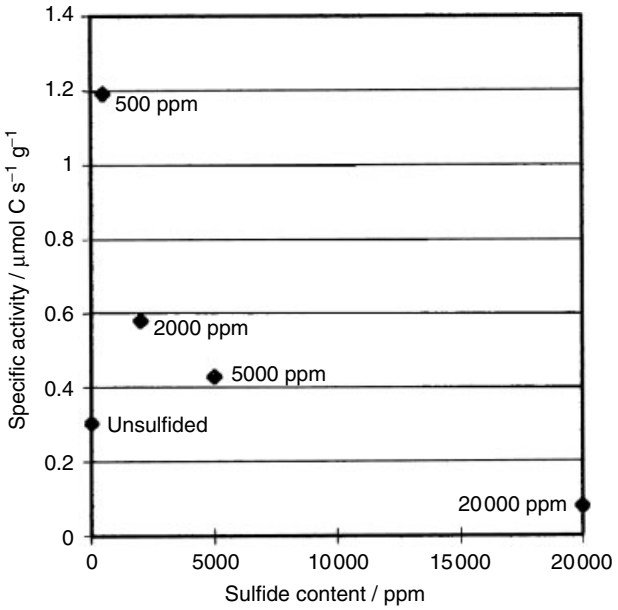

Fig. 17 Specific activity for Fischer–Tropsch synthesis on sulfided Fe catalysts at 523 K. Sulfur was added in the form of Na_2S (500–20 000 ppm). Reactions were performed at 8×10^5 Pa pressure and $H_2/CO = 2$. The data were collected over 4 days [117].

B Co-Based Catalysts Cobalt-based catalysts have been used in FT synthesis because of their advantage of having lower activity for the WGS reaction that causes low carbon usage. Another advantage of Co catalysts is the increase in the secondary chain growth from α-olefins [119, 120]. The FT synthesis rate over Co catalysts is independent of Co dispersion and the type of support, such as TiO_2, SiO_2, and Al_2O_3 [121]. In studies of molecular sieves (MCM-41 and -48) as supports for Co catalysts [122, 123], higher CO conversion rates were found, which were attributed to the increased number of active sites. The CO conversion rate and yield of higher hydrocarbons (C_{5+}) were increased with increasing Co loading up to 5 wt.%, but remained nearly the same at higher Co content [123].

a Electropositive Modifiers Coville and coworkers [124–126] found that boron increased the interaction of cobalt oxides with titania (TiO_2) by decreasing the reducibility of Co catalysts and the number of active sites. The overall FT rate decreased with increasing B loading, but the TOF did not change significantly. Small amounts of B increased the ratio of olefin/paraffin products, and this reached a maximum at 0.1 wt.% of B. Larger amounts (1.5 wt.% B) shifted the product selectivity towards lower hydrocarbons. Various precursors of B were tested, but these did not affect the TOF, even though they affected the CO conversion rates. Boron was effective in forming sulfur-resistant Co catalysts [125].

Alkali modifiers are effective for producing oxygenated products. For example, the addition of alkali metals (Li, Na, K, Rb and Cs) to Co/SiO_2 catalysts improved the selectivity for C_2 oxygenated products such as ethanol, acetaldehyde, and acetic acid [127].

Noble metal promoters generally improve the overall rate of FT synthesis over Co-based catalysts [128–130]. The catalytic performances of unpromoted and promoted Co catalysts on Al_2O_3 and SiO_2 supports are listed in Table 3. Small amounts of noble metals improved the overall FT rate on Co catalysts on both supports. On Co/Al_2O_3 catalysts, Pt showed the highest CO conversion rates, while Pd showed the lowest FT activity. Pt and Ru improved the selectivity for higher hydrocarbons. On Co/SiO_2 catalysts, Ru showed the highest activity while Pt had the lowest. Pd-promoted catalysts enhanced the CH_4 selectivity on both supports. Only Ru improved the turnover frequency of the catalyst and this was attributed to a higher Co dispersion and a larger number of Co sites.

Tab. 3 Performance of noble metal-promoted Co catalysts supported on SiO_2 and Al_2O_3. The reaction conditions for Co/Al_2O_3 catalysts were 503 K, 2.0 MPa, and $H_2/CO = 2$ [128], and those for Co/SiO_2 catalysts were 513 K, 1.0 MPa and $H_2/CO = 2$ [129]

Catalyst	*Co loading/ wt.%*	*Noble metal loading/wt.%*	*CO conversion/%*	*CH_4 selectivity/%*	*C_{5+} selectivity/%*
Co/Al_2O_3	12		6.4	27.5	52.2
$Co-Ru/Al_2O_3$	12	0.5	58.3	15.5	67.4
$Co-Pd/Al_2O_3$	12	0.5	33.1	24.2	57.5
$Co-Pt/Al_2O_3$	12	0.5	61.3	15.6	68.0
Ru/Al_2O_3		0.5	8.4	5.2	92.8
Co/SiO_2	10		33.5	8.89	
$Co-Ru/SiO_2$	10	0.2	72.3	8.81	
$Co-Pd/SiO_2$	10	0.2	57.9	17.76	
$Co-Pt/SiO_2$	10	0.2	49.5	13.78	
Ru/SiO_2		0.2	2.5	4.81	

Other metal modifiers, such as Zn [131, 132], Zr [133], and Mo [134], have been tested in Co catalysts. Zn increased the overall activity for FT synthesis, while product selectivity depended on catalyst preparation. Zr also improved the activity and selectivity for higher hydrocarbons. Mo-promoted $Co/K/SiO_2$ showed a large improvement in the olefin/paraffin ratio, and improved the selectivity for higher hydrocarbons by suppressing methane formation.

b Electronegative Modifiers Sulfur is a known poison; for example, continuous exposure of H_2S (0.5–6 ppm) on Co/SiO_2 catalysts resulted in reduced FT catalytic activity [116]. Sulfur can also affect the selectivity, and adding sulfur (up to S : Co ratio = 0.15) to Co catalysts increased the selectivity for higher hydrocarbons (C_4–C_8). It has also been reported that small amounts of sulfur may increase the FT activity on Co catalysts, as observed for Fe catalysts. Curtis et al. [135], in studies of Co supported on TiO_2 and SiO_2, found that small amounts (100 ppm) of S increased the CO adsorption strength and enhanced the catalytic activity for FT synthesis. As the sulfur content was increased, the formation of hydrocarbons on the catalysts decreased. Li and Coville [125] have reported that small amounts (<200 ppm) of S did not affect significantly the activity and selectivity of Co/TiO_2 catalysts, whereas large amounts (>500 ppm) led to severe poisoning.

5.3.4.3.5 **Ammonia Synthesis** About 3% of the world's energy consumption is used to carry out NH_3 (ammonia) synthesis, which is used primarily for the production of fertilizers. Historically, the Haber–Bosch process has been used to synthesize ammonia from N_2 in air and H_2 over iron-based catalysts that are promoted with metal oxides. The reaction can be written as

$$N_2 + 3H_2 \longrightarrow 2\,NH_3 \quad \Delta H^0_{298} = -92.22\ \text{kJ mol}^{-1} \tag{8}$$

The large N_2 bond dissociation energy requires the use of a catalyst in order to carry out the reaction in a feasible process. Even at the reaction temperatures of 700–850 K which are needed to produce a suitable rate, the thermal equilibrium is small ($<1 \times 10^{-4}$) due to the negative entropy change. Therefore, high pressure ($2–4 \times 10^7$ Pa) is also needed to produce NH_3.

Commercial iron catalysts are promoted with metal oxides, such as Fe_3O_4, K_2O, CaO, and Al_2O_3. Ammonia synthesis has been reviewed extensively, and many details of the promoters and poisons of iron catalysts for ammonia synthesis were reviewed in the First Edition of this Handbook. Here, the primary discussion will be centered on recently developed Ru-based catalysts that function at lower temperatures and pressures. Figure 18 shows, graphically, the superior catalytic activity of Ba- and Cs-promoted Ru/MgO catalysts over iron catalysts at low temperatures [136].

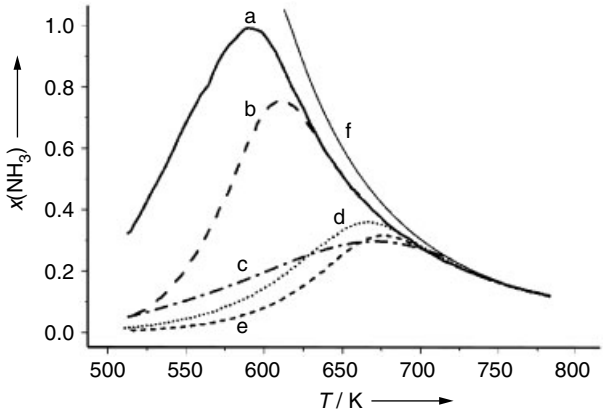

Fig. 18 Catalytic activity of promoted Ru catalysts and industrial Fe catalysts. (a) Ba-promoted Ru/MgO; (b) Cs-promoted Ru/MgO; (c) Fe catalyst; (d, e) unpromoted Ru/MgO; (f) mole fractions of ammonia at equilibrium. Reactions were conducted at a total pressure of 0.1 MPa with $p_{N_2} : p_{H_2} = 1 : 3$ [136].

In general, the following elementary steps can describe ammonia synthesis.

Each of these reactions has been investigated extensively using surface analytical techniques on well-defined surfaces. Hydrogen dissociative adsorption occurs readily on iron single-crystal surfaces with a reasonably high initial sticking coefficient ($S_o \sim 0.1$) and with an adsorption energy of 60 to 100 kJ mol^{-1} [137]. The rate-determining step in ammonia synthesis is nitrogen dissociative adsorption, which occurs on iron surfaces with a very low sticking coefficient of ($S_o < 10^{-5}$) in the order Fe(111) > Fe(100) > Fe(110) [138, 139]. Molecularly chemisorbed N_2(a) has not been observed on Ru surfaces above 300 K, unlike on iron surfaces, and therefore the N_2 dissociative adsorption step can be simplified on Ru into: $N_2(g) \leftrightarrows 2N(a)$ [140].

A Summary of Iron Ammonia Synthesis Catalysts Ammonia synthesis over iron single crystal surfaces occurs

$$H_2(g) \leftrightarrow 2H(a)$$
$$N_2(g) \leftrightarrow N_2(a) \leftrightarrow 2N(a)$$
$$N(a) + H(a) \leftrightarrow NH(a)$$
$$NH(ad) + H(a) \leftrightarrow NH_2(a)$$
$$NH(ad) + H(a) \leftrightarrow NH_3(a) \leftrightarrow NH_3(g)$$

Scheme 2

References see page 1620

with activities in the order of Fe(111) > Fe(211) ≫ Fe(100) > Fe(210) ≫ Fe(110) [141]. This order was attributed to the concentration of C_7 sites in which Fe atoms have seven nearest neighbors [142]. In contrast to experimental results, theoretical calculations have shown that the nitrogen adsorption energy on Fe(100) was higher than Fe(111) and (110) [143, 144]. Al_2O_3 is often used as a structural modifier for stabilizing iron particles during reduction. Alumina was found to increase the activity of Fe(110) by forming $FeAl_2O_4$ under water vapor and to maintain the high activity of restructured iron particles [145].

Potassium is a good promoter for iron-based catalysts. K adatoms on Fe single crystals increased the N_2 sticking coefficient by two orders of magnitude (as shown in Fig. 19), and decreased the activation energy for N_2 dissociation [146, 147]. K also increased the heat of N_2 molecular adsorption by ~40 kJ mol^{-1}. Adding oxygen on K-promoted Fe catalysts decreased the K-promoting effect. Nonetheless, oxygen stabilized the catalyst surprisingly by preventing K desorption from the catalyst [148]. Adding K to Fe(111) and Fe(100) surfaces did not alter the activation energy for ammonia synthesis. It was suggested that K contributed to desorbing the NH_3 product and opening sites for N_2 dissociative adsorption [149, 150]. High pressure was necessary to improve the ammonia conversion on K-promoted Fe/Al_2O_3 catalysts over unpromoted catalysts [151].

Oxygen, H_2O, CO, and CO_2 are each reversible poisons of iron catalysts [152, 153]. For example, oxygen reduced ammonia synthesis rates presumably by destroying C_7 sites, whereas sulfur is an irreversible poison and remains on the catalyst surface. Chlorine also acts as an irreversible poison, and forms volatile iron halides to reduce activity and increase sintering [154, 155].

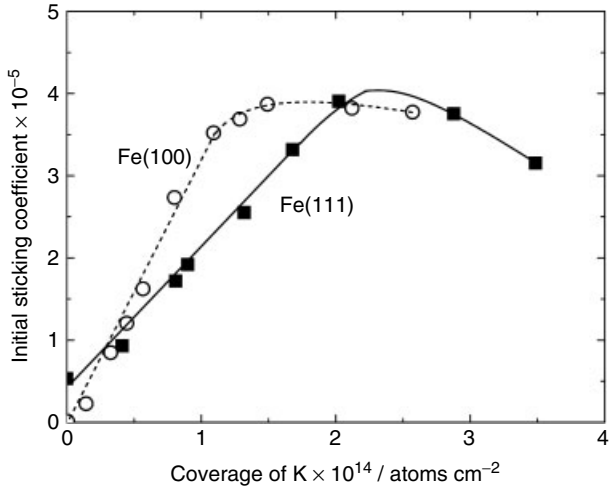

Fig. 19 Initial sticking coefficient for N_2 dissociative adsorption as a function of K coverage on Fe(111) (■) and Fe(100) (○) surfaces at 430 K. (Data adapted from Ref. [147].)

B Ruthenium Catalysts for Ammonia Synthesis

a Active Phase and Structural Modifiers As the rate-determining step in ammonia synthesis, N_2 adsorption has been studied on Ru(0001), $(10\bar{1}0)$, and $(11\bar{2}1)$ single-crystal surfaces [140, 156–161]. The initial sticking coefficient was very small ($S_o \sim 10^{-12}$) at 300 K and almost independent of surface orientation [156]. In comparison, N_2 initial sticking coefficients measured on Ru/Al_2O_3 and Ru/MgO catalysts were 10^{-15} and 10^{-13}, respectively [162]. Dosing excited N_2 molecules (produced by an ionization gauge in ultra-high vacuum, not in line of sight of the sample) increased S_o to ~10^{-6} [140]. The activation energy (E_d) for N_2 dissociation on Ru(0001) was estimated from surface-science experiments to be 190 to 210 kJ mol^{-1} [140, 163]; although theoretical calculations have reported the value to be 135 kJ mol^{-1} [164, 165].

Chorkendorff and coworkers [166, 167] investigated the effect of Ru step sites on N_2 dissociation with experiments and DFT calculations. These authors found that step sites were dominating the N_2 dissociation on Ru(0001). Moreover, the initial sticking coefficient varied with temperature, and could be written as $S_o = 10^{-5.4\pm0.7} \exp(-36 \pm 5 \text{ kJ mol}^{-1} R^{-1} T^{-1})$, giving a value of 2×10^{-12} at 300 K. Blocking step sites with 0.01 monolayer of Au caused S_o to decrease dramatically, by 14 orders of magnitude, at 300 K. As shown in Fig. 20, the activation barrier on step sites is much smaller than terrace sites. In addition, Cao et al. [168] calculated N_2 dissociation on small Ru clusters, and found that steps on the Ru clusters exhibited high activity for N_2 activation and an ensemble of five Ru atoms was the active site. N_2 dissociation on 11 atom clusters showed a two-step process, but only a single-step process on 15- and 21-atom

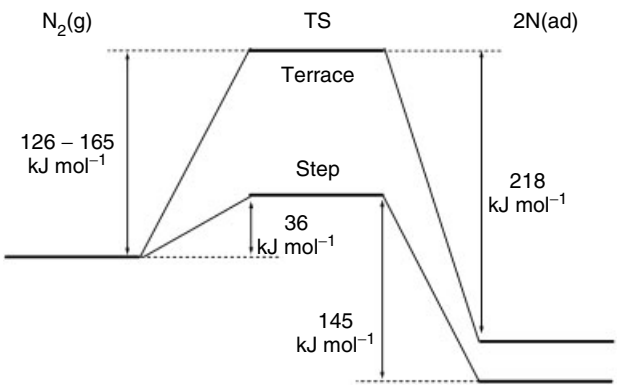

Fig. 20 Dissociation and desorption barriers for N_2 on Ru(0001) [167].

clusters. The N_2 activation energies were calculated as 92 kJ mol^{-1} for 11-atom clusters, and 29 and 42 kJ mol^{-1} for 15- and 21-atom clusters, respectively.

Early studies [169, 170] showed that pure Ru powder was inactive for NH_3 synthesis. On Ru(0001) at 598–898 K, in studies conducted by Dahl et al. [171], the overall activation energy for NH_3 synthesis was estimated as 101 kJ mol^{-1}, with a TOF of 0.02 s^{-1} at 673 K. However, Rosowski et al. [172] reported smaller values at 673 K, namely TOF = 6.5×10^{-3} s^{-1} on Ru/Al_2O_3 and 3.7×10^{-3} s^{-1} on Ru/MgO (see Table 4). The activation energies were also smaller on these supported catalysts, at 69 and 70 kJ mol^{-1} for Ru/MgO and Ru/Al_2O_3, respectively.

Several theoretical calculations of ammonia synthesis were conducted on Ru(0001) [173–175]. Rod et al. [173] suggested that ammonia synthesis might proceed via molecular N_2 and hydrogen ($H^+ + e^-$) at low temperature and pressure. Zhang et al. [174], in calculations of the stepwise nitrogen hydrogenation to NH_3 on Ru(0001), found that the activation barrier for NH hydrogenation was very large (123 kJ mol^{-1}), and similar to that for N_2 dissociation. Logadóttir and Nørskov [175], by investigating all of the elementary steps in ammonia synthesis on Ru(0001) from N_2 and H_2 in the gas phase, showed that step sites were much more reactive than terrace sites.

As supports have been shown to play a key role, various types of support [e.g., MgO, Al_2O_3, $MgAl_2O_4$, Si_3N_4, carbon, and boron nitride (BN)] have each been investigated [136, 176–181]. Unfortunately, direct comparison between these results is difficult because the reaction conditions used were not the same. Modified carbon supports are used in current, commercially available catalysts. Kowalczyk et al. [177, 182, 183] prepared Ru catalysts supported on commercial active carbon and precalcined at 2173 K under a helium atmosphere. Carbon supports with a high surface area and porosity led to a higher dispersion of ultrafine Ru particles, which was attributed to the presence of ultrasmall nanopores (<3 nm diameter). Liang et al. [178] investigated Ru dispersed on different carbon supports, namely activated carbon, activated carbon fiber, and carbon molecular sieves, and found that activated carbon generated the largest amount of ammonia synthesis, whilst activated carbon fiber showed the highest TOF value.

Szmigiel et al. [176] showed that Ru supported on a Mg–Al spinel ($MgO-Al_2O_3$) had better catalytic activity than on MgO alone. In studies by Jacobsen et al. [179], catalytic activities were of the order: $Ru/MgAl_2O_4$ > $Ru/C \gg Ru/Si_3O_4$ (see Fig. 21a). The activation energies were 60, 110–112 and 131 kJ mol^{-1} for $Ru/MgAl_2O_4$, Ru/C, and Ru/Si_3O_4, respectively. The activity of the $Ru/MgAl_2O_4$ catalyst increased during an initial test run, and this was accompanied by the disappearance of small crystallites (<1 nm). The authors suggested that

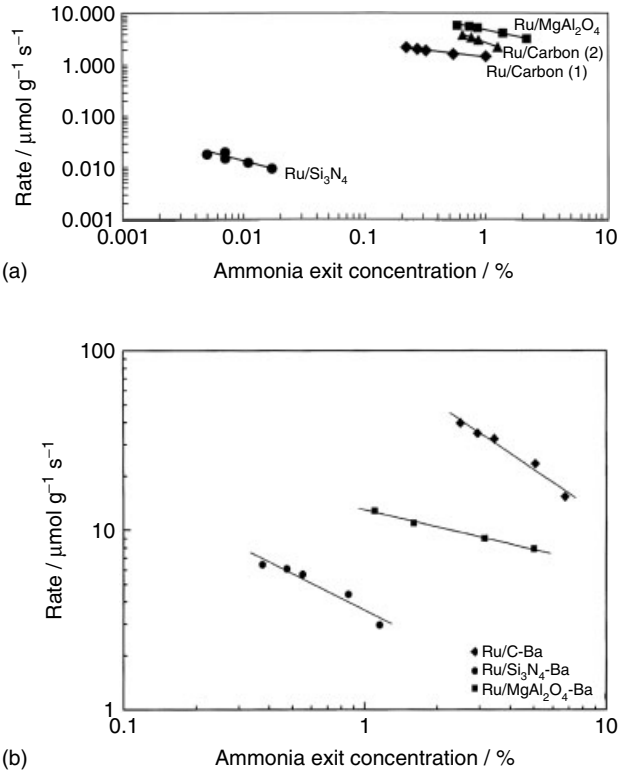

Fig. 21 Catalytic activity of: (a) Ru catalysts supported on C, Si_3N_4 and $MgAl_2O_4$; (b) the same catalysts containing a Ba promoter. Reactions were conducted at 673 K and a pressure of 5×10^6 Pa with $H_2/N_2 = 3$ [179, 181].

a lower limit for the active crystallite size might exist for ammonia synthesis. Hansen et al. [181] investigated Ba-promoted Ru supported on Si_3N_4, $MgAl_2O_4$, and graphitized carbon (C). The activity was measured at 593–713 K and the activity order found to be: Ba–Ru/C > $Ba-Ru/MgAl_2O_4$ > $Ba-Ru/Si_3O_4$ (see Fig. 21b).

Ba-promoted Ru/BN catalysts exhibited significantly higher activity than promoted Ru/C catalysts [180], but the activation energy of 95 kJ mol^{-1} was similar to that for Ba–Ru/C catalysts. The most prominent effect of BN was to increase the stability of the Ba–Ru/BN catalyst, which showed no deactivation after 3500 h at 673 K.

b Metal Modifiers Alkali (K, Cs) and alkaline earth (Ba) metals have been investigated as promoters on Ru catalyst for ammonia synthesis. Forni and coworkers [184, 185] investigated the effect of K, Cs, and Ba promoters on Ru supported on active carbon (C) catalysts. Cs and Ba addition caused higher activity than K-promotion. The order of the promoter effect was: Cs > Ba > K at 703 K and 10^7 Pa with $H_2/N_2 = 1.5$. A mixture of the

References see page 1620

three promoters exhibited even higher activity than the individually promoted catalysts. The highest activity was generated from a Ru catalyst promoted with a mixture of three in an atomic ratio of Ru(4.6 wt.%) : Ba : Cs : K = 1 : 0.6 : 1.0 : 3.4. Raróg et al. [186] also investigated the promoted Ru/C catalysts and the influence of total pressure (see Fig. 22). The activity of the Ba−Ru/C catalyst exhibited a strong dependence on total pressure, whereas Cs- and K-promoted catalysts did not. The best combination for highest catalytic activity could also depend on the pressure, being Ba : Cs : K = 7.5 : 1.25 : 1.0 at 63×10^5 Pa and Ba : Cs : K = 2.75 : 1.45 : 1.0 at 4×10^5 Pa.

Kowalczyk and coworkers [182, 183] probed the effect of K, Cs, and Ba on the stability and reactivity of Ru/C catalysts. The Ba-promoted catalyst was more active and more resistant to overheating than were the K-promoted and unpromoted catalysts. The reactivity of K-promoted catalysts as a function of K content at different reaction temperatures is shown in Fig. 23. Liang et al. [178] pointed out that precursors could affect activity, and that the use of KOH as a precursor was more effective than using KNO_3.

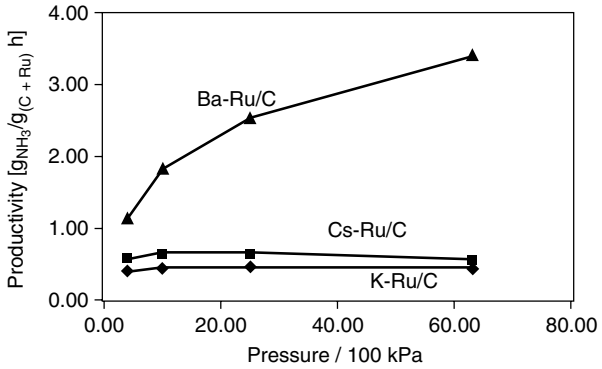

Fig. 22 Promoter effects on the ammonia synthesis activity of Ru/C catalysts at 643 K [186].

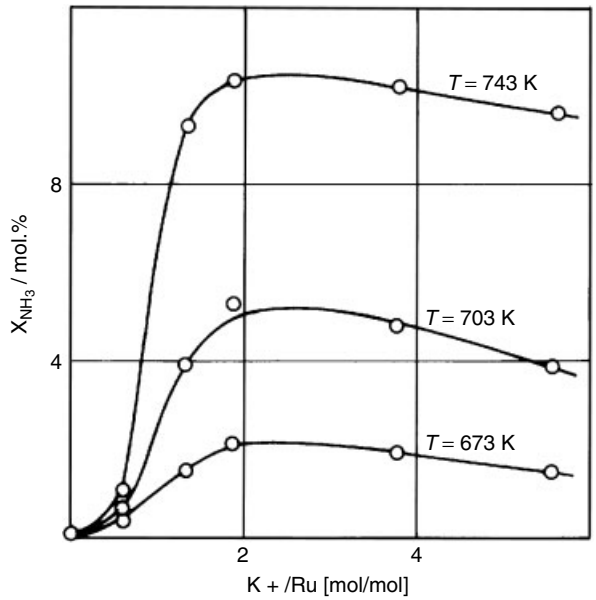

Fig. 23 Activity of a K-promoted Ru/C catalyst as a function of K concentration. Reactions were conducted at 673, 703, and 743 K [182].

Szmigiel et al. [187] prepared Ru catalyst supported on MgO and promoted with Ba and Cs. Ba promotion showed the highest activity for ammonia synthesis, with the ratio of reaction rates being Ba−Ru/MgO : Cs−Ru/MgO : Ru/MgO = 40 : 20 : 1 with synthesis gas of $H_2/N_2/NH_3 = 3 : 1 : 0.05$. Siporin and Davis [188] investigated Ba-, Cs-, and La-promoted Ru/MgO catalysts; hence, La-promoted Ru/MgO had an activity similar to the Ba-promoted catalyst and threefold larger than Cs-promoted Ru/MgO catalysts (see Table 4).

Barium modification has been probed on catalysts of Ru supported on MgO [136, 176], BN [180, 189], activated carbon [177, 181], Si_3O_4 [181], and $MgAl_2O_4$ [176, 181]. Overall, Ba caused higher activities than the unpromoted catalyst and iron catalysts. Also, Rosowski et al [172] investigated alkali promoters on Ru/MgO and Ru/Al_2O_3 catalysts, along with different precursors. The activity for ammonia synthesis was in the order of: Cs_2CO_3−Ru/MgO > $CsNO_3$−Ru/MgO > Ru/MgO > Ru/K−Al_2O_3 > Ru/Al_2O_3 (see Table 4).

c Poisoning Modifiers Electronegative elements (S, N, O, and Cl) present as impurities in the activated carbon used as a support are reported to reduce the catalytic activity of Ru catalysts. Zhong and Aika [190] removed these contaminants successfully by treating activated carbon with hydrogen at 473 K for 5 h. Such hydrogen treatment did not interfere with other promoter action in improving the activity.

5.3.4.4 Case Studies of the Fundamental Basis of Modifier Action in Catalysis

In the following section, four examples of the importance of additives in modifying the performance of catalysts are briefly discussed as case studies, and the results of these specific systems considered in greater detail. These systems provide textbook-like examples of the action of promoters and poisons in several classes of catalysis; moreover, in some cases they provide additional insight into the specific mechanism of this action and the origin of the influences of promoters and poisons.

5.3.4.4.1 Ca promotion in Pd/SiO_2 Catalysts for Methanol Synthesis Methanol is an important chemical feedstock and liquid fuel. Additional attention has resulted recently from interest in developing a direct methanol fuel

Tab. 4 Catalytic activity for ammonia synthesis over Ru and promoted Ru catalysts. Values for the turnover frequency (TOF) were calculated by extrapolation to 673 K utilizing the observed activation energies

Catalyst	*Ru/wt.%*	*Atom ratio of promoter/Ru*	*TOF/s^{-1}*	*Pressure/ bar*	*E_a/ kJ mol^{-1}*	*Reference*
Ru(0001) single crystal			2×10^{-2}	2.1	101	[171]
Ru powder			1.6×10^{-3}	0.78	117	[262]
Ru/MgO	1.7		3.8×10^{-3}	20.7	107	[263]
Ru/MgO	5		8.8×10^{-3}	20	78	[172]
Ru/MgO	5		3.7×10^{-3}	1	69	[172]
Ru/MgO	5		8.8×10^{-3}	20	78	[172]
Ru/Al_2O_3	5		6.5×10^{-4}	1	70	[172]
Ru/Al_2O_3	5		2.5×10^{-3}	20	76	[172]
Cs−Ru/MgO	1.6	0.95	3.4×10^{-2}	20.7	111	[263]
Cs−Ru/MgO	2	1	2×10^{-2}	1	113	[264]
Cs−Ru/MgO	5	1	4.8×10^{-2}	20	109	[172]
$Cs-Ru/Al_2O_3$	5	3	2.8×10^{-3}	1	103	[172]
$Cs-Ru/Al_2O_3$	5	3	3.6×10^{-3}	20	101	[172]
Cs−Ru/C	3	1	1.6×10^{-1}	63		[265]
Cs−Ru/C	9.1	0.3	2.5×10^{-1}	63		[265]
Cs−Ru/C	20	0.1	2.8×10^{-1}	63		[265]
Cs−Ru/C	9.1	1.5	5.0×10^{-1}	63		[186]
Ba−Ru/MgO	1.4	1.26	1.5×10^{-1}	20.7	96	[263]
Ba−Ru/MgO	3.3			20	77	[136]
Ba−Ru/MgO	5.0	0.14	8.8×10^{-1}	63		[176]
Ba−Ru/MgO	10.0	0.07	8.4×10^{-1}	63		[176]
Ba−Ru/C	9.1	0.43	8.3×10^{-1}	63		[186]
La−Ru/MgO	1.6	0.97	1.1×10^{-1}	20.7	86	[263]
K−Ru/C	9.1	2.6	4.0×10^{-1}	63		[186]

cell. Methanol has been produced historically from syngas ($H_2 + CO$) formed from natural gas or coal. Environmental concerns involving greenhouse gases have provided incentives for the synthesis of methanol from CO_2 rather than CO in syngas. Methanol synthesis involves the following main reactions:

$$CO + H_2 \longrightarrow CH_3OH \qquad \Delta H^0_{298} = -90.64\text{kJ mol}^{-1} \tag{9}$$

$$CO_2 + 3H_2 \longrightarrow CH_3OH + H_2O \qquad \Delta H^0_{298} = -49.47\text{kJ mol}^{-1} \tag{10}$$

$$CO + H_2O \longrightarrow CO_2 + H_2 \qquad \Delta H^0_{298} = -41.17\text{kJ mol}^{-1} \tag{11}$$

Methanol is synthesized commercially from syngas mostly using a $CuO/ZnO/Al_2O_3$ catalyst at 573 K at a pressure of 5 to 10×10^6 Pa. Some early reports showed that Pd/SiO_2 catalysts exhibited higher catalytic activity for methanol synthesis than commercial Cu-based catalysts when the support contained impurities [191, 192]. Later, Prins and coworkers [192–195] found that Pd/SiO_2 promoted by one of these impurities, calcium, showed high activity and selectivity (>90%) for CO hydrogenation to methanol; this Ca promoter action is briefly discussed below.

For context, Kikuzono et al. [196], in investigations of the effect of alkali metals on Pd catalysts, found that the methanol synthesis depended strongly on the alkali metal used, in the order: Li > Na ≫ K > Rb > Cs. Alkaline earth metal promotion of Pd/SiO_2 catalysts was reported by Shen and coworkers [197], who observed that CO hydrogenation produced exclusively methanol even at atmospheric pressure with activities in the order of: Mg > Ca > Sr > unpromoted > Ba-promoted catalysts. Investigations by Gotti and Prins [192, 193] probed the effect of Ca promotion and the influence of Pd precursors used in preparing catalysts. Pd supported on ultrapure SiO_2 shows almost no activity for CO hydrogenation (see Table 5). Ca-doped catalysts prepared from Pd precursors of $PdCl_2$, $Pd(NO_3)_2$ and $Pd(NH_3)_4(NO_3)_2$ all exhibited higher activity than Pd supported on pure SiO_2. Catalysts prepared from $PdCl_2$ and $Pd(NH_3)_4(NO_3)_2$ had higher total activity than catalysts from $Pd(NO_3)_2$, and this was related to metal dispersion. Catalysts prepared from $Pd(NO_3)_2$ showed higher methanol selectivity, which suggested that methanol synthesis was unaffected by

References see page 1620

Tab. 5 Catalytic properties of Pd/SiO_2 catalysts prepared from different precursors with and without Ca promotion. Reactions were conducted at 553 K and 2.5 MPa with $CO/H_2 = 2$ at a 770 h^{-1} space velocity for 24 h [192]

Precursor	*Ca/Pd*	*Activity/ $mmol_{CO}$ mol_{Pd}^{-1} s^{-1}*	*TOF/ 10^{-3} s^{-1}*	*Selectivity/%*		
				CH_4	*C_{2+}*	*C_{1-OXO}*
$Pd(NO_3)_2$	0	0.2	8.6	12.0	2.3	85.7
$Pd(NH_3)_4(NO_3)_2$	0	0.4	0.5	54.7	3.7	41.6
$PdCl_2$	0	0.6	0.3	71.8	8.9	19.3
$Pd(NO_3)_2$	0.04	2.2	109.3	0.4	0.2	99.4
$Pd(NH_3)_4(NO_3)_2$	0.04	7.2	25.4	0.1	0.1	99.8
$PdCl_2$	0.04	6.9	22.8	0.6	0.1	99.3

metal dispersion. Ca addition (Ca/Pd = 0.04) on these catalysts increased not only the total activity of the catalysts by one order of magnitude compared to the unpromoted catalysts, but also the selectivity of methanol above 99% on all catalysts, independent of precursors.

Gotti and Prins [193], while investigating a wide range of metal promoters (Li, Na, K, Rb, Cs, Mg, Ca, Sr, Ba, Mn, Zn and La) on Pd/SiO_2 and Pd/Al_2O_3 catalysts for CO and CO_2 hydrogenation to methanol, found that La promotion gave the largest activity for methanol formation on Pd/SiO_2. Li showed the best activity among alkali metals, even though all alkali metals additives gave lower activities than alkaline earth metals. The acid–base properties of the additives were shown to be related to the catalytic activity. Figure 24 shows the rate enhancement for C_{1-OXO} (methanol and dimethyl ether) formation as a function of the electronegativity (EN) of promoters in the hydrogenation of CO and CO_2. Additives with low and high cation EN had little affect on the activity, whereas those with moderate cation EN and amphoteric character (La) greatly enhanced the rate. Among alkali-earth metals, Ca was the best promoter for methanol synthesis. In addition, the effect of Ca loading on Pd/SiO_2 catalysts was probed by Prins and coworkers [193, 194]; their results are listed in Table 6. A small amount of calcium dramatically improved the catalytic activity and selectivity for C_{1-OXO} species. Increasing the Ca loading (>0.05 Ca/Pd) increased not only the total activity of the catalysts and the selectivity for C_{1-OXO} species, but also the fraction of methanol among C_{1-OXO} species.

Sellmer et al. [198] investigated the mechanism of methanol synthesis on Ca-promoted Pd/SiO_2 catalysts utilizing X-ray photoelectron spectroscopy (XPS) and secondary ion mass spectrometry (SIMS). Li-, Ca-, and La-doped Pd/SiO_2 catalysts were tested for methanol synthesis, and the activity was found to be in the order Li < Ca < La. SIMS revealed that the reaction intermediates surface-bound formate and methoxy species were located on the silica support, and not on the Pd particle surface. XPS investigations on pure SiO_2 doped with Ca (10 wt.%)

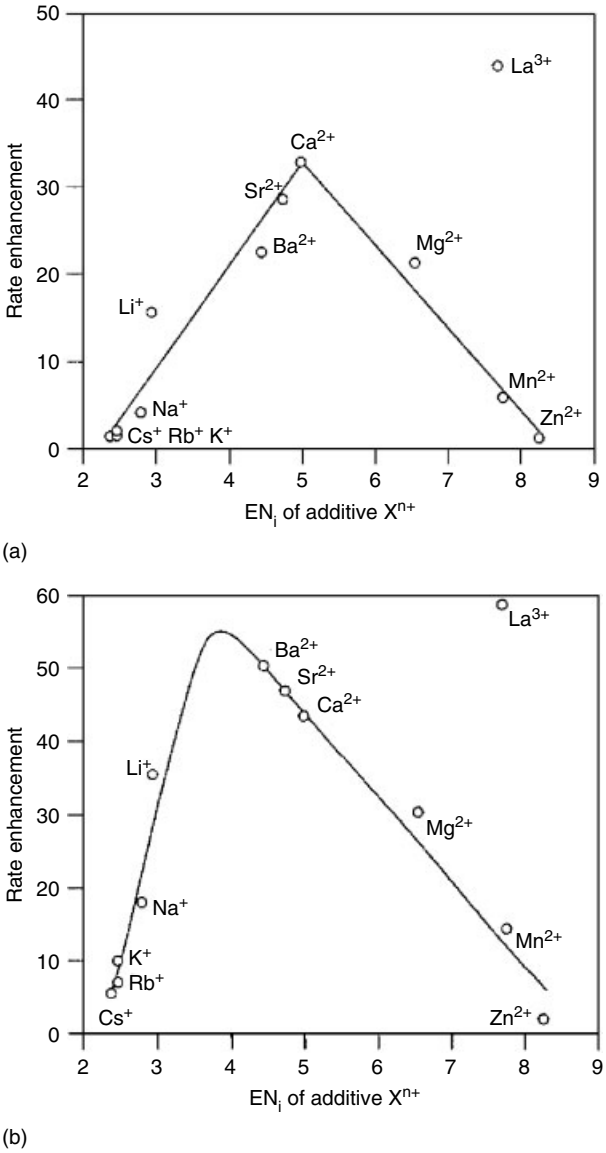

Fig. 24 Rate enhancement for C_{1-OXO} formation in the hydrogenation of CO (a) and CO_2 (b) as a function of the electronegativity (EN) of the additive cation (X) [193].

Tab. 6 Catalytic properties of $Ca/Pd/SiO_2$ catalysts prepared from $Pd(NH_3)_4(NO_3)_2$ and $Ca(NO_3)_2$ precursors. The Pd loading was 4.5 atom%. Reactions were conducted at 553 K and 2.5 MPa with $CO/H_2 = 2$ at a 770 h^{-1} space velocity for 24 h [194]

Ca/Pd	*Activity/mmol$_{CO}$ mol$_{Pd}^{-1}$ s^{-1}*	*TOF/ 10^{-3} s^{-1}*	*Selectivity/%*			*MeOH/ DME*[a]
			C_{1-OXO}	CH_4	C_{2+}	
0	0.26	0.8	29.0	59.1	4.3	1.3
0.004	0.29	1.3	62.8	24.9	1.9	1.1
0.02	1.08	4.9	90.1	4.7	0.4	7.3
0.05	2.90	13.2	92.9	2.1	0.2	59
0.10	3.98	20.2	93.7	1.6	0.3	200
0.20	4.53		92.8	1.6	0.2	120
0.30	4.61	22.9	93.5	1.6	0.2	270
0.50	4.86	23.5	93.7	1.6	0.3	440

[a] Ratio of methanol/dimethyl ether.

showed that the Si $2p$ and O $1s$ peaks shifted to lower values by 0.6 and 0.9 eV, respectively. In contrast, K and Cs addition did not induce these shifts, which correlated with the low catalytic activity for these promoters and the location of Ca on the SiO_2 support. However, Gusovius et al. [194] investigated the location of Ca promoters on supported Pd/SiO_2 catalysts using transmission electron microscopy (TEM), and these studies indicated that Ca addition did not affect the distribution of Pd particle sizes. Based on results from H_2 and CO chemisorption and temperature-programmed reduction (TPR), these authors concluded that Ca preferentially was localized on the Pd particles rather than on the SiO_2 support. Furthermore, it was suggested that Ca, when located on or near Pd particles, was responsible for the high selectivity and high activity for C_{1OXO} production. Infrared (IR) spectra of CO adsorbed on $Ca-Pd/SiO_2$ catalysts suggested that Ca preferred to be on (111) planes rather than (100). Figure 25 shows the IR spectra of CO adsorbed on a Pd/SiO_2 catalyst that was promoted with Ca. Band α represents atop-bonded CO, and bands β and γ are from bridge-bonded CO on (100) and (111) sites, respectively. All three bands are shifted by adding Ca to the catalysts, indicating an electronic effect on the Pd. Evidently, the presence of Ca on (111) sites caused the disappearance of band γ in the IR spectrum from the $Ca/Pd = 0.5$ catalyst.

In order to better investigate the electronic effects of a Ca dopant on Pd particles, Jerdev et al. [199] investigated Ca addition on a Pd(111) surface in ultrahigh vacuum by XPS. The addition of 0.33 ML Ca on Pd(111) at 300 K caused the Pd 3d peak to shift by 0.15 eV to higher values. When the surface was heated, it began to form an alloy at 700 K, and the Pd $3d$ peak began to shift back to lower binding energy. A Ca−Pd alloy was formed by annealing to 1100 K, characterized by a Pd $3d$ peak at the same binding energy, as on clean Pd(111). This

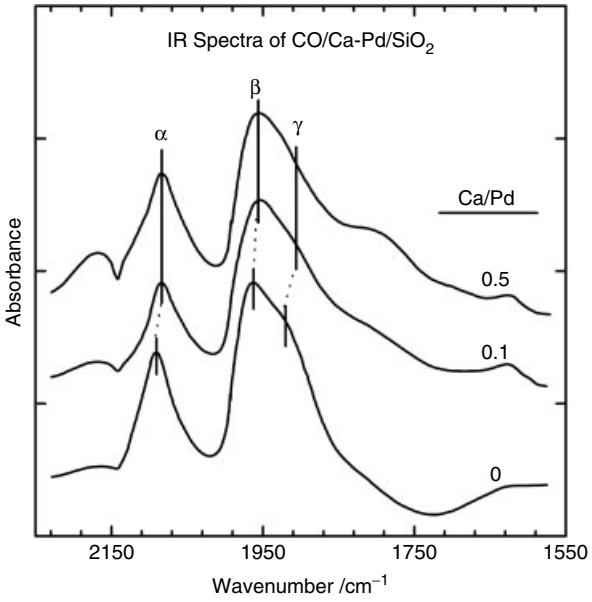

Fig. 25 Infrared spectra of CO adsorbed at room temperature on Pd/SiO_2 catalysts promoted with Ca. The spectra were recorded at a CO pressure of 2200 Pa [194].

indicates that alloyed calcium did not grossly affect the electronic structure of Pd. Nonetheless, the CO energy on the Ca−Pd alloy was increased by 29 kJ mol^{-1}. Further IR studies of CO adsorption and measurement of catalytic rates and selectivities on such model surfaces would reveal additional insights.

5.3.4.4.2 **Direct Formation of Hydrogen Peroxide** Hydrogen peroxide (H_2O_2) is one of the strongest oxidizing agents commercially available in aqueous solution. It has

References see page 1620

been used in many chemical reactions to carry out oxidation, reduction, substitution, molecular addition, and decomposition. Uses of H_2O_2 are on the rise because of environmental concerns leading to the replacement of chlorine-based bleaching with cleaner peroxide chemistry. Industrial H_2O_2 is synthesized almost exclusively by the indirect oxidation of H_2, based on anthrahydroquinone autoxidation in the Riedl–Pfeiderer process. However, the economics of manufacture might be improved by the use of a heterogeneous catalyst and a direct synthesis route.

The so-called direct synthesis of H_2O_2 using Pd catalysts has been investigated and patented [200–205]. The net reaction is

$$H_2 + O_2 \longrightarrow H_2O_2 \quad \Delta H^0_{298} = -187.78 \text{ kJ mol}^{-1} \tag{12}$$

Krishnan et al. [206] reported on a fundamental study of direct H_2O_2 synthesis on Pd supported on porous hafnium phosphate viologen phosphate (HfPOPV(X)). The optimal medium was found to be methanol with sulfuric acid, and 3.5 M H_2O_2 was achieved in 50 h of operation at atmospheric pressure. Choudhary and coworkers [207–213] developed a novel membrane catalyst system, and tested several supports for Pd catalysts along with the promotional effects of halide anions. Lunsford and coworkers [214–220] focused on Pd supported on SiO_2 catalysts and the dramatic influence of halide ions on the selectivity for H_2O_2 formation. The chemistry of this reaction will be discussed briefly below.

A Pd Catalysts for Direct H_2O_2 Synthesis Even though several patents show reasonable activity for Pd catalysts, their use in direct H_2O_2 synthesis has not been commercialized due to the highly explosive nature of H_2/O_2 gas mixtures, and poor selectivity. Choudhary and coworkers [207] developed a novel membrane catalyst for synthesizing H_2O_2 by using a composite Pd–membrane catalyst to separate H_2 from O_2 in the liquid reaction medium in the reactor. Membrane reactors are able to function at higher pressures (2.5 MPa) than conventional slurry reactors, and also exhibit a higher activity for H_2 conversion. A large increase was observed in the H_2O_2 selectivity on Pd thin films deposited on a Pd−Ag/Al_2O_3 membrane. The high selectivity and activity was attributed to molecular O_2 reactions with H atoms permeating through the Pd on the membrane.

Dissannyake and Lunsford [214, 215] investigated the role of colloidal Pd in direct H_2O_2 synthesis from H_2 and O_2 in the aqueous phase. Colloidal Pd was provided by $PdCl_2$ or a Pd/SiO_2 catalyst that was dissolved by HCl in aqueous solution. The rate of H_2O_2 formation is proportional to the amount of active colloidal Pd. Colloidal Pd prepared from the Pd/SiO_2 catalyst showed the highest rate, whereas the Pd/SiO_2 catalyst itself was almost inactive. On the other hand, the largest amount of H_2O_2 was 0.7 wt.%, obtained from colloidal Pd from $PdCl_2$ for the reaction conducted with $O_2/H_2 = 2$ at 298 K and 10^5 Pa for 23 h. An oxygen isotope ($^{16}O_2/^{18}O_2$) investigation using Raman spectroscopy showed that O_2 did not dissociate during H_2O_2 reaction.

The effect of the support on H_2O_2 synthesis was also investigated by Choudhary and coworkers [208, 210]. Fluorinated (F^-), chlorinated (Cl^-) or sulfated (SO_4^-) Al_2O_3, ZrO_2, CeO_2, ThO_2, Y_2O_3, Ga_2O_3 were tested as supports for a PdO catalyst with fluorination or sulfation in a pure water or 0.02 M H_2SO_4 medium. The Pd catalysts were oxidized in air and the PdO phase was confirmed using X-ray diffraction. The H_2O_2 yield over the supported catalyst was calculated by the amount of H_2O_2 formed divided by the amount of H_2 in the gas feed. The yield was in the order: $Ga_2O_3 > ThO_2 > F-\gamma\text{-}Al_2O_3 > F-CeO_2 > Cl-\gamma\text{-}Al_2O_3 > PdO/CeO_2 > F-ZrO_2 \geq SO_4-ZrO_2 > F-Y_2O_3 > F-ThO_2 > F-Ga_2O_3 \geq SO_4-Ga_2O_3 > Y_2O_3 > \gamma\text{-}Al_2O_3 \geq ZrO_2$. Reduction of PdO to metallic Pd decreased the selectivity of H_2O_2 formation and increased H_2O_2 decomposition activity.

The acidic medium also played a key role in promoting H_2O_2 formation on Pd catalysts. The H_2O_2 yield on oxidized Pd supported on zeolites was increased by the acidic medium in the order: HCl (13.3%) > HNO_3(8.2%) > H_3PO_4(7.7%) > $H_2SO_4 \approx HClO_4$ (7.2%) [209]. H_2O_2 decomposition over a Pd/C catalyst was examined at different concentrations of H_2SO_4 and reaction temperatures [221]. The decomposition rate of H_2O_2 was decreased by raising the H_2SO_4 concentration, and increased by raising the reaction temperature. The results of investigations conducted by Han and Lunsford [218, 219] of direct H_2O_2 formation over Pd/SiO_2 catalysts in a reaction medium of ethanol or water with H_2SO_4 or HCl are gathered in Fig. 26. Ethanol solutions provided a better productivity of H_2O_2 over Pd catalysts. The H_2SO_4/ethanol medium showed the highest H_2O_2 production, whilst H_2SO_4/H_2O showed the least. The high activity of the H_2SO_4/ethanol medium was attributed to the formation of acetate ions, which blocked the Pd ensembles needed for H_2O_2 dissociation.

B Promotion Effects of Halide Anions H_2O_2 synthesis can be considered as occurring in four coupled reactions, as shown in Scheme 3 [220]. In the scheme, only reaction I results in H_2O_2 formation, while the others lead to H_2O formation. It has been suggested that halide ions affect several of these individual reactions. Hutchings et al. [222] suggested that Br^- ions suppressed reaction II, hydrogen combustion. Burch and Ellis [223] proposed that halide

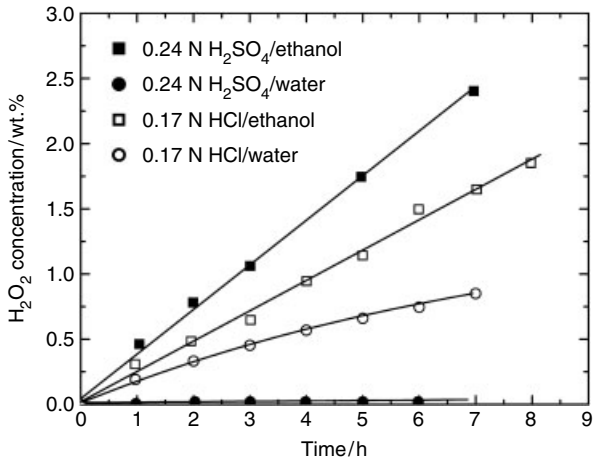

Fig. 26 Catalytic H_2O_2 formation in ethanol and water solutions acidified with 0.24 N H_2SO_4 and 0.17 N HCl. Data are given for H_2SO_4/ethanol (■), H_2SO_4/water (●), HCl/ethanol (□), and HCl/water (○). (Adapted from Ref. [219].)

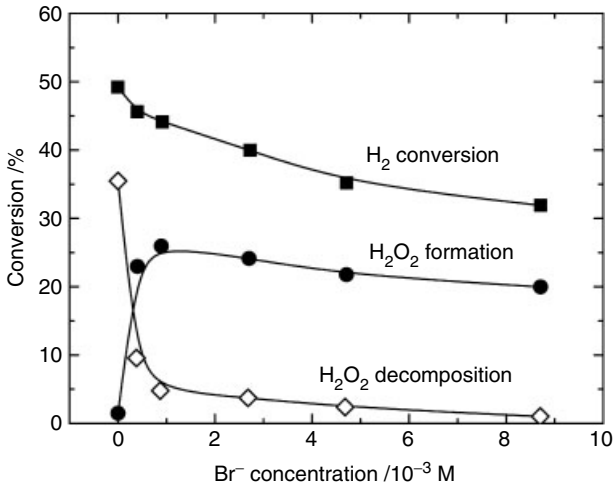

Fig. 27 Effect of Br^- concentration on H_2 conversion (■), H_2O_2 formation (●) and H_2O_2 decomposition (◊) over a Pd/Al_2O_3 catalyst at 300 K acidified with 0.03 M H_2PO_4 [212]. (1 M = 10^3 mol m^{-3}.)

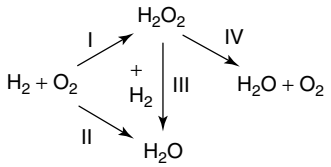

Scheme 3

ions may suppress reaction IV, H_2O_2 dissociation, by blocking neighboring sites or altering the electronic structure of Pd.

Choudhary and Samanta [212] investigated the effects of halide ions (F^-, Cl^-, Br^- and I^-) on H_2O_2 synthesis over Pd catalysts, and found that only Cl^- and Br^- ions acted as promoters and dramatically improved the selectivity for H_2O_2 formation. Figure 27 shows, graphically, the effect of Br^- ion concentration on H_2 conversion, H_2O_2 formation and H_2O_2 decomposition over Pd/Al_2O_3 catalysts acidified with 0.03 M H_2PO_4. A small concentration of Br^- promotes H_2O_2 formation and suppresses its decomposition, whereas larger amounts of Br^- slightly decreased the activity for H_2O_2 formation. The promoting effects of halides were primarily attributed to the inhibition of H_2O_2 decomposition (reaction IV) and hydrogenation (reaction III).

Lunsford and coworkers [218, 220] also studied the effects of chloride and bromide ions on direct H_2O_2 synthesis over Pd/SiO_2 catalysts. A small amount (4×10^{-4} M) of Cl^- ion enhanced the H_2O_2 formation rate; this promoting effect was attributed to the inhibition of O—O bond breaking in O_2 and H_2O_2 molecules. However, relatively large amounts of Br^- (1×10^{-3} M) decreased the net formation of H_2O_2, while large amounts of Cl^- were less effective in decreasing H_2O_2 formation.

Thus, it is clear that halide ions have a dramatic effect on the selectivity for H_2O_2 formation. It seems reasonable that this occurs by inhibiting the breaking of the O—O bond on the Pd surface, both in O_2 and in H_2O_2. However, the origin of the halide effect, either geometric or electronic in nature, remains unclear. Additional spectroscopic information concerning this system is desperately needed, but classical surface science studies are of little use for probing this environment.

5.3.4.4.3 **Methane Reforming on Au—Ni Catalysts** Renewed interest in methane reforming has been sparked by the need to generate hydrogen for polyelectrolyte membrane (PEM)-based and solid-oxide fuel cells, which require clean hydrogen without CO impurities. The reaction of methane reforming was discussed earlier in the chapter, but it useful to consider here gold-modified Ni catalysts for methane reforming. This catalyst provides a good example of how surface-science experiments and theoretical calculations can provide fundamental understanding and lead to new catalysts.

A Recent Studies on Ni Catalysts for Methane Reforming Choudhary and Goodman [224, 225] attempted to produce CO-free hydrogen from methane steam reforming over Ni/ZrO_2 catalysts, by proposing a two-step process for the reaction as shown in Scheme 4.

References see page 1620

Step I: $CH_4 \rightarrow C(a) + CH_n(a) + (2 - {}^{n}/_{2})H_2$

Step II: $C(a) + CH_n(a) + H_2O \rightarrow CO_2 + (2 + {}^{n}/_{2})H_2$

Scheme 4

Methane decomposes into surface carbon, C(a), and adsorbed hydrocarbons, $CH_n(a)$, in Step I, while C(a) and $CH_n(a)$ are removed by steam gasification in Step II. Thus, the net reaction can be written as $CH_4 + 2H_2O \rightarrow CO_2 + 4H_2$. Cycles of introducing CH_4 first and H_2O later on a Ni/ZrO_2 catalyst at 648 K were repeated and the output gases analyzed. Most of the surface carbon formed in Step I was removed by H_2O in Step II. Surface carbon exists in three forms on Ni: (i) a highly reactive carbidic; (ii) an unreactive graphitic; and (iii) a reactive amorphous form. The unreactive graphitic carbon could not be removed by steam; moreover, removal was found to be more difficult at high temperature, indicating that the active surface carbon converts to an unreactive carbon species at high temperature. Inactive carbon was accumulated on the surface with repeated reactions. The methane conversion was ~75% at 648 K, with a pulse of 1.65 mL of 5% CH_4 in He.

Rakass et al. [226] investigated methane reforming on unsupported Ni powder catalysts. These Ni catalysts had an open filamentary structure with irregular fractal-like surfaces and a high external/internal surface ratio. CH_4 conversion was increased and coke deposition decreased significantly by a decrease in the $CH_4 : H_2O$ ratio, where thermodynamic equilibrium is achieved at $CH_4 : H_2O = 1 : 2$. The CH_4 conversion was $98 \pm 2\%$ at 973 K, and no coke was generated during steam reforming. The products of methane reforming were H_2, CO, and CO_2. The onset of hydrogen production occurred at 598 K, and this reached a plateau above 823 K. The amount of CO increased with higher reaction temperatures, whereas the amount CO_2 decreased with increasing temperature.

Matumura and Nakamori [227] tested several supports (SiO_2, Al_2O_3, and ZrO_2) for Ni catalysts. The activity of the Ni/SiO_2 catalyst reduced with H_2 at 773 K decreased upon Ni oxidation by steam during methane reforming. Ni/Al_2O_3 was not easily reduced with H_2 at 773 K, and was inactive for methane reforming. Ni/ZrO_2 catalysts exhibited the best activity for methane reforming at 773 K. The OH(a) on the catalyst reacted readily with methane to form H_2 and CO_2, indicating that surface hydroxyl plays a key role in the mechanism of methane steam reforming. Roh et al. [228, 229] also investigated $Ce-ZrO_2$, ZrO_2, CeO_2, $MgAl_2O_4$, and Al_2O_3 as catalyst supports for Ni, and found that Ni (15 wt.%)/$Ce-ZrO_2$ showed the best activity and stability for methane reforming at 1023 K with $CH_4/H_2O = 0.33$. Although the concentration of NiO_x played an important role in the catalytic activity and stability, reduced Ni metallic sites were considered active for methane reforming reactions. Catalysts with a 12 wt.% Ni loading on $Ce-ZrO_2/Al_2O_3$ exhibited the highest catalytic activity and stability of methane reforming at 1023 K with $CH_4/H_2O = 1$.

B Methane Reforming on Au-Modified Ni Catalysts

Despite the high activity of Ni catalysts for methane reforming, the reaction deposits inactive carbon that is built up on the surface after extensive or repeated reactions [225]. As surface carbon build-up is initiated on step sites of Ni on the catalyst, there is a need to control the concentration of step sites in order to develop carbon-resistant catalysts. Recently, gold emerged as a potentially useful site blocker for Ni catalysts [230].

Holmblad et al. [231, 232] first investigated Au deposition on a Ni(111) surface and its effect on the reaction of CH_4, CO and deuterium (D_2). Au atoms formed a surface alloy in the topmost Ni layer and were distributed almost at random (see Fig. 28) [230]. The gold atoms appeared as dark spots, and the Ni atoms adjacent to these Au atoms appeared brighter than the other Ni atoms, indicating that the Au atoms had modified the electronic and geometric structures of the Ni surface. Increasing the Au coverage of the Au/Ni(111) alloy decreased the initial sticking coefficient of methane and reduced the saturation coverage of surface carbon. An increase in the Au coverage led to a

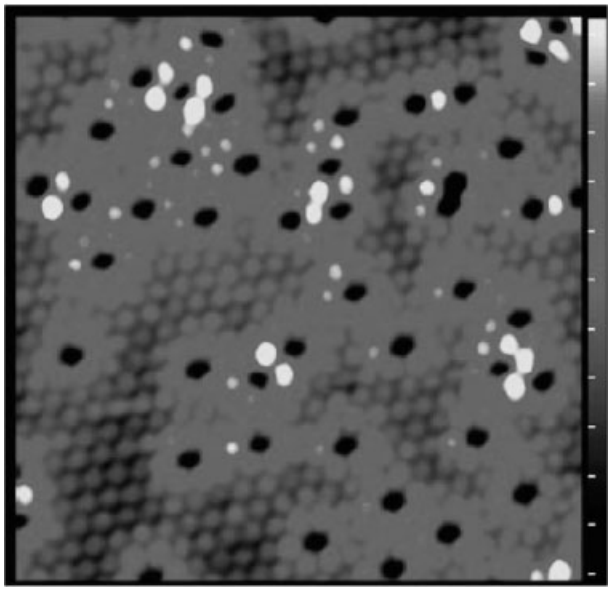

Fig. 28 Scanning tunneling microscopy (STM) image of a Ni(111) surface modified with 7% of one monolayer of Au. Au atoms appear as black dots and Ni atoms as bright spots [230].

decrease in CO and D_2 coverage and in their desorption energies.

Bengaard et al. [2] used DFT to estimate the energy of a Ni(211) surface in which Au atoms replaced Ni atoms at the step edge or terrace. A lower energy was calculated for Au atoms replacing Ni atoms at the step edge than at the terrace by 36 kJ mol^{-1}. These authors also calculated the energy for Au atoms dispersed on Ni nanoparticles, predicting that Au atoms were located at the surface of the Ni particles and spread almost evenly over the surface. In addition, DFT calculations of methane dissociation on Au-modified Ni(111) were conducted by Kratzer et al. [233], whose calculations suggested that the CH_3-H dissociation barrier was 100 kJ mol^{-1} on Ni(111). The stable site for CH_3 adsorption was the threefold hollow site on Ni(111), while C−H bond breaking occurred primarily on top of a Ni atom. Alloying Au into the Ni surface increased the dissociation barrier for C−H bond breaking by 16 kJ mol^{-1} for a Ni atom with a Au neighbor atom.

This DFT calculation was tested experimentally by Besenbacher et al. [230] and by Molenbroek et al. [234]. These authors prepared Ni−Au alloy catalysts supported on $MgAl_2O_4$. *n*-Butane was used to test steam-reforming activity as it causes severe graphitic carbon build-up. A 0.3 wt.% Au-modified $Ni/MgAl_2O_4$ catalyst showed the same reactivity as pure $Ni/MgAl_2O_4$ but, as shown in Fig. 29, the Au-modified catalyst did not deactivate whereas the unmodified catalyst deactivated rapidly.

Triantafyllopoulos and Neophytides [235] studied methane dissociative adsorption and partial oxidation on Au-modified Ni supported on yttria-stabilized zirconia (YSZ). The addition of 1 atom% Au (with respect to Ni) to a Ni/YSZ catalyst significantly inhibited the formation of graphitic carbon. It also decreased the rate of methane decomposition and stabilized CH_x species on the surface, so that CH_x(a) hydrogenation to CH_4 occurred at a 100 K higher temperature than with unpromoted Ni catalysts. These authors found that partial oxidation of methane to syngas proceeded by oxidizing CH_x(a) to CH_xO(a), which subsequently dissociated into CO and H_2 at 700 K. The formation of carbidic carbon from methane resulted in complete oxidation to CO_2. Overall, Au additives affect the reactivity of Ni catalysts by slowing down dehydrogenation and hydrogenation of CH_x(a) species on the surface.

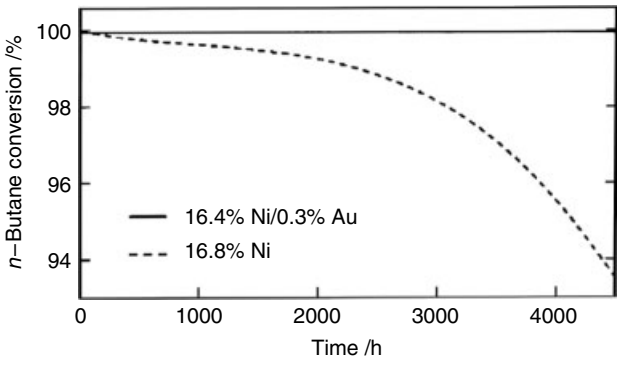

Fig. 29 Conversion of *n*-butane over pure (dashed line) and 0.3 wt.% Au-modified (solid line) $Ni/MgAl_2O_4$ catalysts during steam reforming. The reaction was conducted with 3% *n*-butane, 7% H_2, and 3% H_2O in He carrier gas [230].

5.3.4.4.4 **Oxidative Dehydrogenation of Alkanes** The oxidative dehydrogenation (ODH) of lower alkanes, such as ethane, propane and butane is attractive because of the interest in exploiting alkanes more efficiently. It is much more desirable to form alkenes from oxidative dehydrogenation [Eq. (13)] than to carry out non-selective oxidation to carbon oxides [Eq. (14)] or other side products.

$$C_nH_{2n+2} + 1/2O_2 \longrightarrow C_nH_{2n} + H_2O \quad (13)$$

$$C_nH_{2n+2} + 1/2(3n+1)O_2 \longrightarrow nCO_2 + (n+1)H_2O \quad (14)$$

As described in several recent reviews of ODH of lower alkane on supported metal oxides [236–238], the activity and selectivity for ODH depends on the alkane reactants, the metal oxide catalyst used, and the presence of modifiers. This may be complex, with the same catalyst showing different activities with alkanes of different chain length. Oxides of alkali, alkaline earth, and transition metals have been investigated as supports or additives for the ODH of lower alkanes, with multicomponent catalysts generally giving improved results. Vanadium oxide catalysts have attracted the most attention because of their higher activity and selectivity [239, 240]. Vanadia supported catalysts have shown interesting catalytic properties which depend on the preparation, on the V loading, on additives, and on the nature of the supports. The effects of alkali additives on the ODH reaction are briefly discussed here, and several other influential factors as examples of promoters in oxide catalysis, will be summarized.

A Effects of Supports, Loading, and Preparation Since the first reports in 1988 on propane and *n*-butane oxidative dehydrogenation on vanadium supported on MgO [241, 242], many subsequent studies have resulted in a substantially deeper understanding of the vanadium oxide catalyst system [243, 244]. It is commonly accepted that tetrahedral V species are the active sites for alkane ODH. However, the detailed structure of tetrahedral V species is under debate. Isolated VO_4 tetrahedra [245, 246] and V_2O_7 units [247–249] with oxygen atoms bridging two V atoms have been suggested to be the main active

References see page 1620

structures for alkane ODH selectivity. Since isolated VO_4 tetrahedra do not have bridging oxygen atoms – which are considered to have weaker bonding to V than the other O atoms – these species seem preferable to carry out dehydrogenation reaction. In contrast, V_2O_7 contains bridging O atoms that can be readily removed, and these labile oxygens promote the oxidation reactions to produce O-containing products.

Nieto and coworkers [250, 251] reported that catalytic activity for vanadia supported on Al_2O_3 increased with as the V loading was raised (from 0 to 6.3 wt.%), and selectivity for alkene formation was observed to be maximal at 3–4 wt.% V loading (see Fig. 30). The catalyst with octahedral V^{5+} species showed higher catalytic activity, whereas the catalyst with tetrahedral V^{5+} produced a higher yield of alkene. Vanadium was mainly tetrahedral V^{5+} at less than 15 wt.% V loading, whereas octahedral V^{5+} and V_2O_5 species dominated at higher V contents.

ODH of propane was performed over vanadia catalysts supported on Al_2O_3, MgO, TiO_2, and ZrO_2 [252, 253]; their activities are listed in Table 7. Vanadia supported on TiO_2 exhibits a higher activity than other supports, which appear in the order of $TiO_2 \gg ZrO_2 > Al_2O_3 > MgO$. On the other hand, the V_2O_5/Al_2O_3 catalyst showed the highest selectivity of propane dehydrogenation to propene. The reducibility of the catalyst was seen to correlate with the acid–base character of the supports.

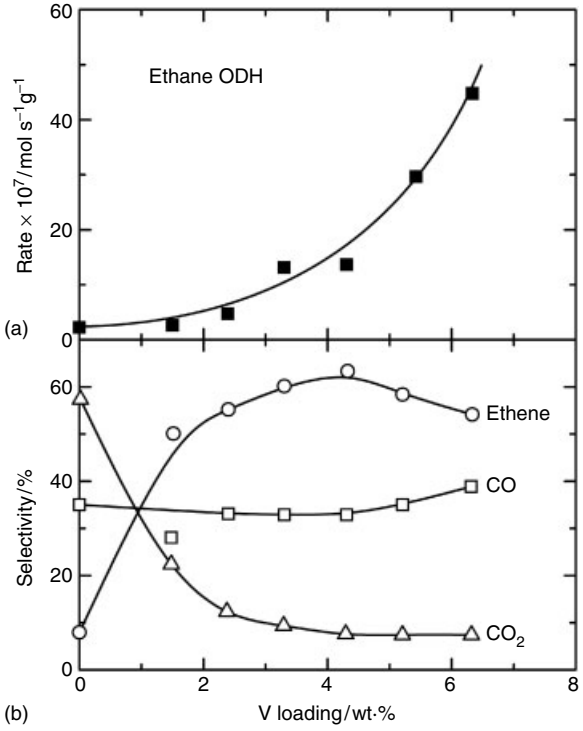

Fig. 30 Effects of loading on VO_x/Al_2O_3 catalysts. (a) Rate of ethane oxidative dehydrogenation (ODH); (b) selectivity for ethene, CO and CO_2. Reaction temperatures were 773 K for (a) and 843 K for (b) [250].

B Effect of Alkali Metal Additives on Vanadia Catalysts

The promotion by alkali metals (Li, Na, K, Cs) of oxidative dehydrogenation of alkanes over vanadium catalysts causes overall larger changes in the selectivity of alkenes than on activity, and their effects are larger for the ODH of higher alkanes. For example, Lemonidou et al. [252] investigated the effect of Li, Na, and K addition to V/Al_2O_3 catalysts using propane ODH as a test reaction. Propane conversion decreased with addition of alkali metals in the order: unpromoted > Li > Na > K (see Table 8). The varying effect was attributed to the basicity of the alkali metal and blocking of active sites by alkali metals. In contrast, the selectivity of producing propene was increased with addition of alkali metals, and the increase of propene selectivity was seen to be independent of the nature of the alkalis. Grabowski and

Tab. 7 Oxidative dehydrogenation of propane over V-based catalysts and pure supports. The V_2O_5 content of the V-containing catalysts was 4 wt.%. Reactions were conducted at 773 K [252]

Catalyst	C_3H_8 *conv./%*	*Selectivity/%*		*SSAc/* $\mu mol_{C_3H_8}$ m^{-2} s^{-1}	C_3H_6 *productivity/* $kg_{C_3H_8}$ kg_{cat}^{-1} h^{-1}
		C_3H_6	CO_x		
MgO	1.5	11.4	88.6	0.003	
V/MgO	25.6	24.8	74.2	0.042	0.15
Al_2O_3	2.5	41.2	58.8	0.002	
V/Al_2O_3	20.3	39.8	60.2	0.035	0.40
TiO_2	6.9	45.4	54.6	0.020	
V/TiO_2	30.4	22.8	77.0	1.200	1.43
ZrO_2	4.5	10.1	89.9	0.007	
V/ZrO_2	33.1	17.1	82.5	0.150	0.28

SSAc = specific surface activity.

Tab. 8 Activity and selectivity of propane oxidative dehydrogenation over alkali-promoted V/Al_2O_3 catalysts. The wt.% of Li, Na and K in the catalysts was 0.165, 0.320, and 0.500, respectively [252]

Catalyst	*Temp./K*	C_3H_8 *conv./%*	*Selectivity/%*	
			C_3H_6	CO_x
V/Al_2O_3	723	13.7	49.7	50.3
	773	30.8	28.8	71.2
$Li-V/Al_2O_3$	723	7.5	73.7	26.3
	773	23.9	49.6	50.4
$Na-V/Al_2O_3$	723	6.2	77.3	22.7
	773	20.2	50.7	49.3
$K-V/Al_2O_3$	723	5.7	80.2	19.8
	773	16.9	57.2	42.8

coworkers [254, 255] studied the effects of Li, K, and Rb on V/TiO_2 catalysts, and found that the total activity for propane ODH decreased with alkali addition in the order: unpromoted > Li > K > Rb. Yield and selectivity of the propene product increased in the opposite order, but this was attributed to the increase in basicity and decrease in acidity of the promoted catalysts.

Nieto and coworkers [256, 257] also studied the effect of potassium on V/Al_2O_3 catalysts for the ODH of ethane and *n*-butane. The addition of K decreased the reducibility of V species and the number of active sites. K decreased the selectivity of ethene production during ethane ODH reaction, but increased the selectivity of C_4-alkene from *n*-butane ODH (Fig. 31). Studies were also carried out for the ODH of 1-butene on the V/Al_2O_3 catalyst, with and without a K promoter. Vibrational spectroscopy showed that the reaction intermediates were different on the unpromoted and promoted catalysts: O-containing species were present on the unpromoted catalyst, whereas butadiene was observed on the K-promoted catalyst. Potassium effects on V/SiO_2 and V/MgO catalysts also have been investigated by Grzybowska and coworkers [258, 259]. The addition of K to V/SiO_2 catalysts decreased the activity of propane ODH by a factor of 2, and increased the selectivity for propene by a factor of 3. Theoretical calculations of K addition suggested that K transferred electron density to V and O atoms in the active units, and that K was adsorbed onto the units rather than forming a K−O bond. On V/MgO, K promoters did not increase the selectivity of propene from propane conversion. Ethane conversion on V/SiO_2 and V/MgO was affected only slightly by the addition of K.

Mechanistically, in the results for propane ODH over V/TiO_2 catalysts with rubidium promotion, it was found that an Eley–Rideal steady-state adsorption model was more appropriate to explain propane ODH on both unpromoted and Rb-promoted catalysts. The addition of Rb decreased the rate constant for propene formation, and

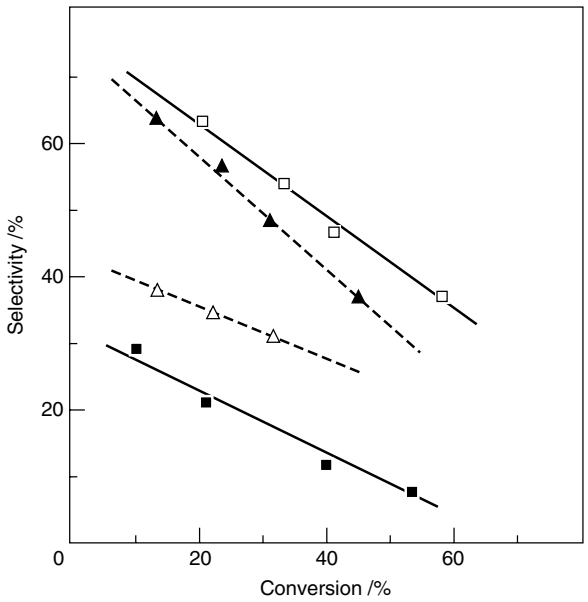

Fig. 31 Influence of the addition of a K promoter on the selectivity for ethene formation (□, Δ) from ethane and for C_4-alkene formation (■, ▲) from *n*-butane oxidative dehydrogenation. Dashed lines indicate data from unpromoted catalysts; solid lines are from K-promoted catalysts [256].

increased the activation energy for subsequent oxidation of propene, which led in turn to an enhancement in the selectivity for propene formation. These changes were assigned to site blocking by Rb on the vanadium phase of the catalyst. Sloczynski [260] also found that the addition of Rb hindered the reduction of the vanadium phase by blocking propane adsorption sites and causing a decrease in the total activity.

Finally, Owens and Kung [261] investigated the effect of cesium addition to V/SiO_2 catalysts for butane ODH. C_4-alkenes and carbon oxides were the main products for the reaction at 793 K, but the addition of Cs led to a significant increase in the selectivity of C_4 alkenes from butane ODH; however, there was no noticeable change in the activation energy or reaction rates. Cs addition also decreased the catalytic activity of *n*-butane conversion.

The redox behavior of these systems, the complex nature of both the structure and composition of all of the phases present, and the difficulty of modeling these catalyst systems and their chemistry – by both experiment and theory – cloud the nature of the promotion and poisoning of these oxide catalysts.

5.3.4.5 Summary

As shown by these few examples and case studies, much progress has been made during the past 30 years in our

References see page 1620

understanding of the mechanisms of action of catalysts and, perhaps more importantly, on how promoters and poisons influence this chemistry. Much of the progress has been achieved by taking a surface-science approach to catalysis, with kinetic and spectroscopic studies of well-defined model systems under controlled conditions being used to isolate individual reactive species, elementary reactions steps, or single types of reactive site. Of course, this approach includes some drastic limitations, namely, the well-known ''pressure gap'' which is often cited between ultrahigh vacuum studies and the high-pressure (up to hundreds of atmospheres) conditions of many working catalysts. Less often cited, but of equal importance, are the temperature and materials gaps between these two situations. The fact that catalysts are such complex, often difficult to prepare reproducibly, multicomponent, and often nanophasic materials, means that this gap will continue to thwart our complete understanding of the promotion and poisoning of catalysts for some time to come. Nonetheless, novel approaches continue to be developed and new tools made available for the characterization and study of both model and practical materials. Indeed, today there is a strong expectation for further developments in our ability to obtaining new experimental data relevant to these issues. For example, electron microscopy, with aberration correction, can operate at sub-Ångstrom resolution to provide the elemental composition of a given, single nanoparticle and resolve the core-shell structure of nanoparticles. Likewise, new synchrotron sources are planned that will radically change the nature and quality of data obtained with techniques such as extended X-ray absorption fine structure (EXAFS). In addition, scanning probe methods, STM and atomic force microscopy, optical spectroscopic methods, together with Raman and IR spectroscopy and sum-frequency generation (SFG), all of which can be used at high pressures, will help to bridge the ''gaps'' in our knowledge. Moreover, rapid advances in theoretical systems and raw computing power will continue to revolutionize the impact of calculations and simulations on modeling to help explain this chemistry. Increasingly today, one hears of success stories based on these approaches for the modification of surface properties and the design of new, highly selective, catalysts.

References

1. J. H. Larsen, I. Chorkendorff, *Surf. Sci. Rep.* **1999**, *35*, 165.
2. H. S. Bengaard, J. K. Norskov, J. Sehested, B. S. Clausen, L. P. Nielsen, A. M. Molenbroek, J. R. Rostrup-Nielsen, *J. Catal.* **2002**, *209*, 365.
3. F. Abild-Pedersen, O. Lytken, J. Engbaek, G. Nielsen, I. Chorkendorff, J. K. Norskov, *Surf. Sci.* **2005**, *590*, 127.
4. M. Andersen, O. Lytken, J. Engbaek, G. Nielsen, N. Schumacher, M. Johansson, I. Chorkendorff, *Catal. Today* **2005**, *100*, 191.
5. R. T. Vang, K. Honkala, S. Dahl, E. K. Vestergaard, J. Schnadt, E. Laegsgaard, B. S. Clausen, J. K. Norskov, F. Besenbacher, *Surf. Sci.* **2006**, *600*, 66.
6. T. P. Beebe, D. W. Goodman, B. D. Kay, J. T. Yates, *J. Chem. Phys.* **1987**, *87*, 2305.
7. I. W. Chen, F. L. Chen, *Ind. Eng. Chem. Res.* **1990**, *29*, 534.
8. A. Golebiowski, K. Stolecki, U. Prokop, A. Kusmierowska, T. Borowiecki, A. Denis, C. Sikorska, *React. Kinet. Catal. Lett.* **2004**, *82*, 179.
9. H. S. Bengaard, I. Alstrup, I. Chorkendorff, S. Ullmann, J. R. Rostrup-Nielsen, J. K. Norskov, *J. Catal.* **1999**, *187*, 238.
10. F. Arena, A. L. Chuvilin, A. Parmaliana, *J. Phys. Chem.* **1995**, *99*, 990.
11. F. Arena, F. Frusteri, A. Parmaliana, *Appl. Catal. A: General* **1999**, *187*, 127.
12. J. D. Lisboa, D. Santos, F. B. Passos, F. B. Noronha, *Catal. Today* **2005**, *101*, 15.
13. M. V. Twigg, *Catalyst Handbook*. 2nd ed., Manson Publishing Ltd., London, 1997, p. 607.
14. J. Sehested, *Catal. Today* **2006**, *111*, 103.
15. Novochinskii, II, C. S. Song, X. L. Ma, X. S. Liu, L. Shore, J. Lampert, R. J. Farrauto, *Energy Fuels* **2004**, *18*, 576.
16. J. R. Rostrup-Nielsen, *J. Catal.* **1984**, *85*, 31.
17. R. Kikowatz, K. Flad, G. Horz, *J. Vacuum Sci. Technol. A. Vac. Surf. Films* **1987**, *5*, 1009.
18. X. D. Jiang, D. W. Goodman, *Appl. Phys. A. Mater. Sci. Process.* **1990**, *51*, 99.
19. X. Jiang, D. W. Goodman, *Catal. Lett.* **1990**, *4*, 173.
20. P. Panagiotopoulou, D. I. Kondarides, *Catal. Today* **2006**, *112*, 49.
21. A. Andreev, V. Idakiev, D. Mihajlova, D. Shopov, *Appl. Catal.* **1986**, *22*, 385.
22. R. L. Keiski, O. Desponds, Y. F. Chang, G. A. Somorjai, *Appl. Catal. A: General* **1993**, *101*, 317.
23. G. P. Van der Laan, A. Beenackers, *Catal. Rev. -Sci. Eng.* **1999**, *41*, 255.
24. E. S. Lox, G. F. Froment, *Ind. Eng. Chem. Res.* **1993**, *32*, 71.
25. G. C. Chinchen, M. S. Spencer, K. C. Waugh, D. A. Whan, *J. Chem. Soc., Faraday Trans. I* **1987**, *83*, 2193.
26. J. E. Kubsh, J. A. Dumesic, *AICHE J.* **1982**, *28*, 793.
27. M. Tinkle, J. A. Dumesic, *J. Catal.* **1987**, *103*, 65.
28. I. Fishtik, R. Datta, *Surf. Sci.* **2002**, *512*, 229.
29. F. Domka, A. Basinska, W. Przystajko, R. Fiedorow, *Surf. Technol.* **1984**, *21*, 101.
30. G. C. Chinchen, R. H. Logan, M. S. Spencer, *Appl. Catal.* **1984**, *12*, 69.
31. G. C. Chinchen, R. H. Logan, M. S. Spencer, *Appl. Catal.* **1984**, *12*, 89.
32. G. C. Chinchen, R. H. Logan, M. S. Spencer, *Appl. Catal.* **1984**, *12*, 97.
33. M. A. Edwards, D. M. Whittle, C. Rhodes, A. M. Ward, D. Rohan, M. D. Shannon, G. J. Hutchings, C. J. Kiely, *Phys. Chem. Chem. Phys.* **2002**, *4*, 3902.
34. D. G. Rethwisch, J. A. Dumesic, *J. Catal.* **1986**, *101*, 35.
35. J. M. T. de Souza, M. D. Rangel, *React. Kinet. Catal. Lett.* **2002**, *77*, 29.
36. J. M. T. de Souza, M. D. Rangel, *React. Kinet. Catal. Lett.* **2004**, *83*, 93.
37. I. L. Júnior, J. M. M. Millet, M. Aouine, M. do Carmo Rangel, *Appl. Catal. A: General* **2005**, *283*, 91.
38. V. Idakiev, D. Mihajlova, B. Kunev, A. Andreev, *React. Kinet. Catal. Lett.* **1987**, *33*, 119.
39. C. Rhodes, B. P. Williams, F. King, G. J. Hutchings, *Catal. Commun.* **2002**, *3*, 381.

40. C. Rhodes, G. J. Hutchings, *Phys. Chem. Chem. Phys.* **2003**, *5*, 2719.
41. Y. Lei, N. W. Cant, D. L. Trimm, *Chem. Eng. J.* **2005**, *114*, 81.
42. Y. Lei, N. W. Cant, D. L. Trimm, *Catal. Lett.* **2005**, *103*, 133.
43. Y. Lei, N. W. Cant, D. L. Trimm, *J. Catal.* **2006**, *239*, 227.
44. G. C. Wang, L. Jiang, Z. S. Cai, Y. M. Pan, X. Z. Zhao, W. Huang, K. C. Xie, Y. W. Li, Y. H. Sun, B. Zhong, *J. Phys. Chem. B* **2003**, *107*, 557.
45. G. C. Wang, L. Jiang, Z. S. Cai, Y. M. Pan, N. J. Guan, Y. Wu, X. Z. Zhao, Y. W. Li, Y. H. Sun, B. Zhong, *Theochem. J.Mol. Struct.* **2002**, *589*, 371.
46. G. C. Wang, L. Jiang, Y. H. Zhou, Z. S. Cai, Y. M. Pan, X. Z. Zhao, Y. W. Li, Y. H. Sun, B. Zhong, X. Y. Pang, W. Huang, K. C. Xie, *Theochem. J. Mol. Struct.* **2003**, *634*, 23.
47. J. Nakamura, J. M. Campbell, C. T. Campbell, *J. Chem. Soc., Faraday Trans.* **1990**, *86*, 2725.
48. M. J. L. Ginés, N. Amadeo, M. Laborde, C. R. Apesteguía, *Appl. Catal. A: General* **1995**, *131*, 283.
49. M. Saito, K. Tomoda, I. Takahara, K. Murata, M. Inaba, *Catal. Lett.* **2003**, *89*, 11.
50. J. G. Wu, M. Saito, *J. Catal.* **2000**, *195*, 420.
51. C. T. Campbell, B. E. Koel, *Surf. Sci.* **1987**, *186*, 393.
52. J. A. Rodriguez, W. D. Clendening, J. M. Campbell, M. Wu, C. T. Campbell, *J. Vac. Sci. Technol. A. Vac. Surf. Films* **1989**, *7*, 2118.
53. J. M. Campbell, J. Nakamura, C. T. Campbell, *J. Catal.* **1992**, *136*, 24.
54. J. A. Rodriguez, W. D. Clendening, C. T. Campbell, *J. Phys. Chem.* **1989**, *93*, 5238.
55. D. S. Newsome, *Catal. Rev. -Sci. Eng.* **1980**, *21*, 275.
56. C. T. Campbell, B. E. Koel, *Surf. Sci.* **1987**, *183*, 100.
57. J. A. Rodriguez, S. Chaturvedi, M. Kuhn, *Surf. Sci.* **1998**, *415*, L1065.
58. I. Alstrup, *J. Catal.* **1995**, *151*, 216.
59. S. Fujita, M. Nakamura, T. Doi, N. Takezawa, *Appl. Catal. A: General* **1993**, *104*, 87.
60. D. W. Goodman, R. D. Kelley, T. E. Madey, J. M. White, *J. Catal.* **1980**, *64*, 479.
61. J. Sehested, S. Dahl, J. Jacobsen, J. R. Rostrup-Nielsen, *J. Phys. Chem. B* **2005**, *109*, 2432.
62. T. Mori, H. Masuda, H. Imai, A. Miyamoto, S. Baba, Y. Murakami, *J. Phys. Chem.* **1982**, *86*, 2753.
63. S. Fujita, H. Terunuma, M. Nakamura, N. Takezawa, *Ind. Eng. Chem. Res.* **1991**, *30*, 1146.
64. T. K. Campbell, J. L. Falconer, *Appl. Catal.* **1989**, *50*, 189.
65. D. E. Peebles, D. W. Goodman, J. M. White, *J. Phys. Chem.* **1983**, *87*, 4378.
66. C. Schild, A. Wokaun, R. A. Koeppel, A. Baiker, *J. Phys. Chem.* **1991**, *95*, 6341.
67. S. Qin, C. W. Hu, H. Q. Yang, Z. S. Su, *J. Phys. Chem. A* **2005**, *109*, 6498.
68. M. Agnelli, M. Kolb, C. Mirodatos, *J. Catal.* **1994**, *148*, 9.
69. M. Agnelli, H. M. Swaan, C. Marquez-Alvarez, G. A. Martin, C. Mirodatos, *J. Catal.* **1998**, *175*, 117.
70. E. B. Pereira, G. A. Martin, *Appl. Catal. A: General* **1994**, *115*, 135.
71. D. W. Goodman, R. D. Kelley, T. E. Madey, J. T. Yates, *J. Catal.* **1980**, *63*, 226.
72. R. D. Kelley, D. W. Goodman, *Surf. Sci.* **1982**, *123*, L743.
73. S. Z. Ozdogan, P. D. Gochis, J. L. Falconer, *J. Catal.* **1983**, *83*, 257.
74. C. H. Bartholomew, C. K. Vance, *J. Catal.* **1985**, *91*, 78.
75. C. K. Kuei, J. F. Lee, M. D. Lee, *J. Mol. Catal.* **1990**, *59*, 333.
76. A. Diaz, D. R. Acosta, J. A. Odriozola, M. Montes, *J. Phys. Chem. B* **1997**, *101*, 1782.
77. C. T. Campbell, D. W. Goodman, *J. Vac. Sci. Technol. A. Vac. Surf. Films* **1983**, *1*, 1265.
78. K. M. Bailey, T. K. Campbell, J. L. Falconer, *Appl. Catal.* **1989**, *54*, 159.
79. I. Alstrup, M. T. Tavares, *J. Catal.* **1993**, *139*, 513.
80. M. T. Tavares, I. Alstrup, C. A. Bernardo, J. R. Rostrup-Nielsen, *J. Catal.* **1996**, *158*, 402.
81. M. Agnelli, C. Mirodatos, *J. Catal.* **2000**, *192*, 204.
82. W. Erley, H. Wagner, *J. Catal.* **1978**, *53*, 287.
83. K. D. Rendulic, A. Winkler, *Surf. Sci.* **1978**, *74*, 318.
84. J. R. Rostrup-Nielsen, K. Pedersen, *J. Catal.* **1979**, *59*, 395.
85. D. W. Goodman, M. Kiskinova, *Surf. Sci.* **1981**, *105*, L265.
86. M. Kiskinova, D. W. Goodman, *Surf. Sci.* **1981**, *108*, 64.
87. F. Fischer, H. Tropsch, *Ber. Deutsch. Chem. Ges.* **1926**, *59*, 830.
88. C. K. Rofer-DePoorter, *Chem. Rev.* **1981**, *81*, 447.
89. A. T. Bell, *Catal. Rev. -Sci. Eng.* **1981**, *23*, 203.
90. J. P. Hindermann, G. J. Hutchings, A. Kiennemann, *Catal. Rev. -Sci. Eng.* **1993**, *35*, 1.
91. M. E. Dry, *Appl. Catal. A: General* **1996**, *138*, 319.
92. A. A. Adesina, *Appl. Catal. A: General* **1996**, *138*, 345.
93. J. A. Amelse, J. B. Butt, L. H. Schwartz, *J. Phys. Chem.* **1978**, *82*, 558.
94. G. B. Raupp, W. N. Delgass, *J. Catal.* **1979**, *58*, 361.
95. J. W. Niemantsverdriet, A. M. Vanderkraan, W. L. Vandijk, H. S. Vanderbaan, *J. Phys. Chem.* **1980**, *84*, 3363.
96. H. B. Zhang, G. L. Schrader, *J. Catal.* **1985**, *95*, 325.
97. R. A. Dictor, A. T. Bell, *J. Catal.* **1986**, *97*, 121.
98. E. S. Lox, G. B. Marin, E. Degrave, P. Bussiere, *Appl. Catal.* **1988**, *40*, 197.
99. K. Rao, F. E. Huggins, V. Mahajan, G. P. Huffman, V. U. S. Rao, *Hyperfine Interact.* **1994**, *93*, 1745.
100. K. Rao, F. E. Huggins, V. Mahajan, G. P. Huffman, V. U. S. Rao, B. L. Bhatt, D. B. Bukur, B. H. Davis, R. J. O'Brien, *Top. Catal.* **1995**, *2*, 71.
101. D. B. Bukur, L. Nowicki, R. K. Manne, X. S. Lang, *J. Catal.* **1995**, *155*, 366.
102. M. D. Shroff, D. S. Kalakkad, K. E. Coulter, S. D. Kohler, M. S. Harrington, N. B. Jackson, A. G. Sault, A. K. Datye, *J. Catal.* **1995**, *156*, 185.
103. D. B. Bukur, X. Lang, D. Mukesh, W. H. Zimmerman, M. P. Rosynek, C. P. Li, *Ind. Eng. Chem. Res.* **1990**, *29*, 1588.
104. Y. Yang, H. W. Xiang, L. Tian, H. Wang, C. H. Zhang, Z. C. Tao, Y. Y. Xu, B. Zhong, Y. W. Li, *Appl. Catal. A: General* **2005**, *284*, 105.
105. W. Ngantsoue-Hoc, Y. Q. Zhang, R. J. O'Brien, M. S. Luo, B. H. Davis, *Appl. Catal. A: General* **2002**, *236*, 77.
106. D. B. Bukur, D. Mukesh, S. A. Patel, *Ind. Eng. Chem. Res.* **1990**, *29*, 194.
107. S. Li, A. Li, S. Krishnamoorthy, E. Iglesia, *Catal. Lett.* **2001**, *77*, 197.
108. A. P. Raje, R. J. O'Brien, B. H. Davis, *J. Catal.* **1998**, *180*, 36.
109. M. S. Luo, R. J. O'Brien, S. Q. Bao, B. H. Davis, *Appl. Catal. A: General* **2003**, *239*, 111.
110. M. S. Luo, B. H. Davis, *Appl. Catal. A: General* **2003**, *246*, 171.
111. J. Yang, Y. C. Sun, Y. Tang, Y. Liu, H. L. Wang, L. Tian, H. Wang, Z. X. Zhang, H. W. Xiang, Y. W. Li, *J. Mol. Catal. A: Chemical* **2006**, *245*, 26.
112. R. J. O'Brien, L. G. Xu, R. L. Spicer, S. Q. Bao, D. R. Milburn, B. H. Davis, *Catal. Today* **1997**, *36*, 325.
113. S. L. Soled, E. Iglesia, S. Miseo, B. A. Derites, R. A. Fiato, *Top. Catal.* **1995**, *2*, 193.

114. R. J. O'Brien, B. H. Davis, *Catal. Lett.* **2004**, *94*, 1.
115. C. H. Zhang, Y. Yang, B. T. Teng, T. Z. Li, H. Y. Zheng, H. W. Xiang, Y. W. Li, *J. Catal.* **2006**, *237*, 405.
116. C. H. Bartholomew, R. M. Bowman, *Appl. Catal.* **1985**, *15*, 59.
117. T. C. Bromfield, N. J. Coville, *Appl. Catal. A: General* **1999**, *186*, 297.
118. B. S. Wu, L. Bai, H. W. Xiang, Y. W. Li, Z. X. Zhang, B. Zhong, *Fuel* **2004**, *83*, 205.
119. H. Schulz, E. Vansteen, M. Claeys, *Top. Catal.* **1995**, *2*, 223.
120. J. Patzlaff, Y. Liu, C. Graffmann, J. Gaube, *Appl. Catal. A: General* **1999**, *186*, 109.
121. E. Iglesia, *Appl. Catal. A: General* **1997**, *161*, 59.
122. J. Panpranot, J. G. Goodwin, A. Sayari, *J. Catal.* **2002**, *211*, 530.
123. H. L. Li, S. G. Wang, F. X. Ling, J. L. Li, *J. Mol. Catal. A: Chemical* **2006**, *244*, 33.
124. J. L. Li, N. J. Coville, *Appl. Catal. A: General* **1999**, *181*, 201.
125. J. L. Li, N. J. Coville, *Appl. Catal. A: General* **2001**, *208*, 177.
126. N. J. Coville, J. Li, *Catal. Today* **2002**, *71*, 403.
127. T. Matsuzaki, T. A. Hanaoka, K. Takeuchi, Y. Sugi, M. Reinikainen, *Catal. Lett.* **1991**, *10*, 193.
128. D. Y. Xu, W. Z. Li, H. M. Duan, Q. J. Ge, H. Y. Xu, *Catal. Lett.* **2005**, *102*, 229.
129. N. Tsubaki, S. L. Sun, K. Fujimoto, *J. Catal.* **2001**, *199*, 236.
130. E. Iglesia, S. L. Soled, R. A. Fiato, G. H. Via, *J. Catal.* **1993**, *143*, 345.
131. N. N. Madikizela, N. J. Coville, *J. Mol. Catal. A: Chemical* **2002**, *181*, 129.
132. N. N. Madikizela-Mnqanqeni, N. J. Coville, *Appl. Catal. A: General* **2004**, *272*, 339.
133. H. F. Xiong, Y. H. Zhang, K. Liew, J. L. Li, *J. Mol. Catal. A: Chemical* **2005**, *231*, 145.
134. H. Chen, A. A. Adesina, *Appl. Catal. A: General* **1994**, *112*, 87.
135. V. Curtis, C. P. Nicolaides, N. J. Coville, D. Hildebrandt, D. Glasser, *Catal. Today* **1999**, *49*, 33.
136. H. Bielawa, O. Hinrichsen, A. Birkner, M. Muhler, *Angew. Chem. Int. Ed.* **2001**, *40*, 1061.
137. F. Bozso, G. Ertl, M. Grunze, M. Weiss, *Appl. Surf. Sci.* **1977**, *1*, 103.
138. F. Bozso, G. Ertl, M. Grunze, M. Weiss, *J. Catal.* **1977**, *49*, 18.
139. F. Bozso, G. Ertl, M. Weiss, *J. Catal.* **1977**, *50*, 519.
140. H. Shi, K. Jacobi, G. Ertl, *J. Chem. Phys.* **1993**, *99*, 9248.
141. D. R. Strongin, J. Carrazza, S. R. Bare, G. A. Somorjai, *J. Catal.* **1987**, *103*, 213.
142. G. A. Somorjai, *Introduction to Surface Chemistry and Catalysis*. Wiley International Publishers: New York, 1994, p. 465.
143. J. J. Mortensen, L. B. Hansen, B. Hammer, J. K. Norskov, *J. Catal.* **1999**, *182*, 479.
144. J. J. Mortensen, M. V. Ganduglia-Pirovano, L. B. Hansen, B. Hammer, P. Stoltze, J. K. Norskov, *Surf. Sci.* **1999**, *422*, 8.
145. D. R. Strongin, G. A. Somorjai, New York: 1991, p. 133.
146. G. Ertl, M. Weiss, S. B. Lee, *Chem. Phys. Lett.* **1979**, *60*, 391.
147. G. Ertl, S. B. Lee, M. Weiss, *Surf. Sci.* **1982**, *114*, 527.
148. Z. Paal, G. Ertl, S. B. Lee, *Appl. Surf. Sci.* **1981**, *8*, 231.
149. S. R. Bare, D. R. Strongin, G. A. Somorjai, *J. Phys. Chem.* **1986**, *90*, 4726.
150. D. R. Strongin, S. R. Bare, G. A. Somorjai, *J. Vac. Sci. Technol. A. Vac. Surf. Film* **1987**, *5*, 824.
151. J. Schütze, W. Mahdi, B. Herzog, R. Schlögl, *Top. Catal.* **1994**, *1*, 195.
152. K. C. Waugh, D. Butler, B. E. Hayden, *Catal. Lett.* **1994**, *24*, 197.
153. K. C. Waugh, D. Butler, B. E. Hayden, *Top. Catal.* **1994**, *1*, 295.
154. W. Arabczyk, U. Narkiewicz, D. Moszynski, *Appl. Catal. A: General* **1996**, *134*, 331.
155. E. Murray, J. Prasad, H. Cabibil, J. A. Kelber, *Surf. Sci.* **1994**, *319*, 1.
156. H. Dietrich, P. Geng, K. Jacobi, G. Ertl, *J. Chem. Phys.* **1996**, *104*, 375.
157. H. Dietrich, K. Jacobi, G. Ertl, *J. Chem. Phys.* **1997**, *106*, 9313.
158. K. Jacobi, H. Dietrich, G. Ertl, *Appl. Surf. Sci.* **1997**, *121*, 558.
159. L. R. Danielson, M. J. Dresser, E. E. Donaldson, J. T. Dickinson, *Surf. Sci.* **1978**, *71*, 599.
160. H. Dietrich, K. Jacobi, G. Ertl, *J. Chem. Phys.* **1996**, *105*, 8944.
161. H. Shi, K. Jacobi, G. Ertl, *J. Chem. Phys.* **1995**, *102*, 1432.
162. O. Hinrichsen, F. Rosowski, A. Hornung, M. Muhler, G. Ertl, *J. Catal.* **1997**, *165*, 33.
163. L. Romm, G. Katz, R. Kosloff, M. Asscher, *J. Phys. Chem. B* **1997**, *101*, 2213.
164. J. J. Mortensen, Y. Morikawa, B. Hammer, J. K. Norskov, *J. Catal.* **1997**, *169*, 85.
165. J. J. Mortensen, B. Hammer, J. K. Norskov, *Phys. Rev. Lett.* **1998**, *80*, 4333.
166. S. Dahl, A. Logadottir, R. C. Egeberg, J. H. Larsen, I. Chorkendorff, E. Tornqvist, J. K. Norskov, *Phys. Rev. Lett.* **1999**, *83*, 1814.
167. S. Dahl, E. Tornqvist, I. Chorkendorff, *J. Catal.* **2000**, *192*, 381.
168. Z. X. Cao, H. L. Wan, Q. N. Zhang, *J. Chem. Phys.* **2003**, *119*, 9178.
169. G. Rambeau, H. Amariglio, *J. Catal.* **1981**, *72*, 1.
170. G. Rambeau, H. Amariglio, *Appl. Catal.* **1981**, *1*, 291.
171. S. Dahl, P. A. Taylor, E. Tornqvist, I. Chorkendorff, *J. Catal.* **1998**, *178*, 679.
172. F. Rosowski, A. Hornung, O. Hinrichsen, D. Herein, M. Muhler, G. Ertl, *Appl. Catal. A: General* **1997**, *151*, 443.
173. T. H. Rod, A. Logadottir, J. K. Norskov, *J. Chem. Phys.* **2000**, *112*, 5343.
174. C. J. Zhang, Z. P. Liu, P. Hu, *J. Chem. Phys.* **2001**, *115*, 609.
175. A. Logadottir, J. K. Norskov, *J. Catal.* **2003**, *220*, 273.
176. D. Szmigiel, W. Rarog-Pilecka, E. Miskiewicz, M. Glinski, M. Kielak, M. Kaszkur, Z. Kowalczyk, *Appl. Catal. A: General* **2004**, *273*, 105.
177. Z. Kowalczyk, S. Jodzis, W. Rarog, J. Zielinski, J. Pielaszek, A. Presz, *Appl. Catal. A: General* **1999**, *184*, 95.
178. C. H. Liang, Z. B. Wei, Q. Xin, C. Li, *Appl. Catal. A: General* **2001**, *208*, 193.
179. C. J. H. Jacobsen, S. Dahl, P. L. Hansen, E. Tornqvist, L. Jensen, H. Topsoe, D. V. Prip, P. B. Moenshaug, I. Chorkendorff, *J. Mol. Catal. A: Chemical* **2000**, *163*, 19.
180. C. J. H. Jacobsen, *J. Catal.* **2001**, *200*, 1.
181. T. W. Hansen, P. L. Hansen, S. Dahl, C. J. H. Jacobsen, *Catal. Lett.* **2002**, *84*, 7.
182. Z. Kowalczyk, J. Sentek, S. Jodzis, E. Mizera, J. Goralski, T. Paryjczak, R. Diduszko, *Catal. Lett.* **1997**, *45*, 65.
183. Z. Kowalczyk, S. Jodzis, W. Rarog, J. Zielinski, J. Pielaszek, *Appl. Catal. A: General* **1998**, *173*, 153.
184. L. Forni, D. Molinari, I. Rossetti, N. Pernicone, *Appl. Catal. A: General* **1999**, *185*, 269.
185. I. Rossetti, N. Pernicone, L. Forni, *Appl. Catal. A: General* **2001**, *208*, 271.
186. W. Rarog, Z. Kowalczyk, J. Sentek, D. Skladanowski, J. Zielinski, *Catal. Lett.* **2000**, *68*, 163.
187. D. Szmigiel, H. Bielawa, M. Kurtz, O. Hinrichsen, M. Muhler, W. Rarog, S. Jodzis, Z. Kowalczyk, L. Znak, J. Zielinski, *J. Catal.* **2002**, *205*, 205.

188. S. E. Siporin, R. J. Davis, W. Rarog-Pilecka, D. Szmigiel, Z. Kowalczyk, *Catal. Lett.* **2004**, *93*, 61.
189. T. W. Hansen, J. B. Wagner, P. L. Hansen, S. Dahl, H. Topsoe, C. J. H. Jacobsen, *Science* **2001**, *294*, 1508.
190. Z. H. Zhong, K. Aika, *J. Catal.* **1998**, *173*, 535.
191. F. Fajula, R. G. Anthony, J. H. Lunsford, *J. Catal.* **1982**, *73*, 237.
192. A. Gotti, R. Prins, *Catal. Lett.* **1996**, *37*, 143.
193. A. Gotti, R. Prins, *J. Catal.* **1998**, *175*, 302.
194. A. F. Gusovius, T. C. Watling, R. Prins, *Appl. Catal. A: General* **1999**, *188*, 187.
195. T. C. Watling, A. F. Gusovius, R. Prins, *J. Catal.* **1999**, *188*, 233.
196. Y. Kikuzono, S. Kagami, S. Naito, T. Onishi, K. Tamaru, *Faraday Discuss.* **1981**, 135.
197. Y. F. Shen, J. T. Li, L. F. Cai, K. H. Huang, *J. Mol. Catal.* **1990**, *59*, 61.
198. C. Sellmer, R. Prins, N. Kruse, *Catal. Lett.* **1997**, *47*, 83.
199. D. I. Jerdev, R. Prins, B. E. Koel, *J. Phys. Chem. B* **2004**, *108*, 14417.
200. W. F. Brill Preparation of hydrogen peroxide 4,661,337, November 18, 1985, 1987.
201. L. W. Gosser Catalytic process for making H_2O_2 from hydrogen and oxygen 4,681,751, April 22, 1985, 1987.
202. L. W. Gosser Hydrogen peroxide method using optimized H+ and Br- concentrations 4,889,705, December 26, 1989, 1989.
203. L. W. Gosser, M. A. Paoli Method for catalytic production of hydrogen peroxide 5,135,731, 1992.
204. L. W. Gosser, J. T. Schwartz Catalytic process for making hydrogen peroxide from hydrogen and oxygen employing a bromide promoter 4,772,458, November 19, 1986, 1988.
205. L. W. Gosser, J. T. Schwartz Hydrogen peroxide production method using platinum/palladium catalysts 4,832,938, May 13, 1988, 1989.
206. V. V. Krishnan, A. G. Dokoutchaev, M. E. Thompson, *J. Catal.* **2000**, *196*, 366.
207. V. R. Choudhary, A. G. Gaikwad, S. D. Sansare, *Angew. Chem. Int. Ed.* **2001**, *40*, 1776.
208. V. R. Choudhary, A. G. Gaikwad, S. D. Sansare, *Catal. Lett.* **2002**, *83*, 235.
209. V. R. Choudhary, S. D. Sansare, A. G. Gaikwad, *Catal. Lett.* **2002**, *84*, 81.
210. A. G. Gaikwad, S. D. Sansare, V. R. Choudhary, *J. Mol. Catal. A: Chemical* **2002**, *181*, 143.
211. V. R. Choudhary, C. Samanta, A. G. Gaikwad, *Chem. Commun.* **2004**, 2054.
212. V. R. Choudhary, C. Samanta, *J. Catal.* **2006**, *238*, 28.
213. V. R. Choudhary, C. Samanta, T. V. Choudhary, *Appl. Catal. A: General* **2006**, *308*, 128.
214. D. P. Dissanayake, J. H. Lunsford, *J. Catal.* **2002**, *206*, 173.
215. D. P. Dissanayake, J. H. Lunsford, *J. Catal.* **2003**, *214*, 113.
216. J. H. Lunsford, *J. Catal.* **2003**, *216*, 455.
217. S. Chinta, J. H. Lunsford, *J. Catal.* **2004**, *225*, 249.
218. Y. F. Han, J. Lunsford, *Catal. Lett.* **2005**, *99*, 13.
219. Y. F. Han, J. H. Lunsford, *J. Catal.* **2005**, *230*, 313.
220. Q. S. Liu, J. H. Lunsford, *J. Catal.* **2006**, *239*, 237.
221. V. R. Choudhary, A. G. Gaikwad, *React. Kinet. Catal. Lett.* **2003**, *80*, 27.
222. P. Landon, P. J. Collier, A. F. Carley, D. Chadwick, A. J. Papworth, A. Burrows, C. J. Kiely, G. J. Hutchings, *Phys. Chem. Chem. Phys.* **2003**, *5*, 1917.
223. R. Burch, P. R. Ellis, *Appl. Catal. B: Environmental* **2003**, *42*, 203.
224. T. V. Choudhary, D. W. Goodman, *Catal. Lett.* **1999**, *59*, 93.
225. T. V. Choudhary, D. W. Goodman, *J. Catal.* **2000**, *192*, 316.
226. S. Rakass, H. Oudghiri-Hassani, P. Rowntree, N. Abatzoglou, *J. Power Sources* **2006**, *158*, 485.
227. Y. Matsumura, T. Nakamori, *Appl. Catal. A: General* **2004**, *258*, 107.
228. H. S. Roh, K. W. Jun, W. S. Dong, J. S. Chang, S. E. Park, Y. I. Joe, *J. Mol. Catal. A: Chemical* **2002**, *181*, 137.
229. H. S. Roh, K. W. Jun, S. E. Park, *Appl. Catal. A: General* **2003**, *251*, 275.
230. F. Besenbacher, I. Chorkendorff, B. S. Clausen, B. Hammer, A. M. Molenbroek, J. K. Norskov, I. Stensgaard, *Science* **1998**, *279*, 1913.
231. P. M. Holmblad, J. H. Larsen, I. Chorkendorff, *J. Chem. Phys.* **1996**, *104*, 7289.
232. P. M. Holmblad, J. H. Larsen, I. Chorkendorff, L. P. Nielsen, F. Besenbacher, I. Stensgaard, E. Laegsgaard, P. Kratzer, B. Hammer, J. K. Norskov, *Catal. Lett.* **1996**, *40*, 131.
233. P. Kratzer, B. Hammer, J. K. Norskov, *J. Chem. Phys.* **1996**, *105*, 5595.
234. A. M. Molenbroek, J. K. Norskov, B. S. Clausen, *J. Phys. Chem. B* **2001**, *105*, 5450.
235. N. C. Triantafyllopoulos, S. G. Neophytides, *J. Catal.* **2006**, *239*, 187.
236. M. A. Banares, *Catal. Today* **1999**, *51*, 319.
237. L. M. Madeira, M. F. Portela, *Catal. Rev.-Sci. Eng.* **2002**, *44*, 247.
238. R. Grabowski, *Catal. Rev.-Sci. Eng.* **2006**, *48*, 199.
239. T. Blasco, J. M. L. Nieto, *Appl. Catal. A: General* **1997**, *157*, 117.
240. E. A. Mamedov, V. C. Corberan, *Appl. Catal. A: General* **1995**, *127*, 1.
241. M. A. Chaar, D. Patel, M. C. Kung, H. H. Kung, *J. Catal.* **1987**, *105*, 483.
242. M. A. Chaar, D. Patel, H. H. Kung, *J. Catal.* **1988**, *109*, 463.
243. H. H. Kung, M. C. Kung, *Appl. Catal. A: General* **1997**, *157*, 105.
244. J. M. L. Nieto, R. Coenraads, A. Dejoz, M. I. Vazquez, The role of metal oxides as promoters of V_2O_5/gamma-Al_2O_3 catalysts in the oxidative dehydrogenation of propane. In *3rd World Congress on Oxidation Catalysis*, 1997, Vol. 110, pp. 443.
245. A. Corma, J. M. L. Nieto, N. Paredes, *J. Catal.* **1993**, *144*, 425.
246. P. M. Michalakos, M. C. Kung, I. Jahan, H. Kung, *J. Catal.* **1993**, *140*, 226.
247. T. Lindblad, B. Rebenstorf, Z. G. Yan, S. L. T. Andersson, *Appl. Catal. A: General* **1994**, *112*, 187.
248. D. Sie Hew Sam, V. Soenen, J. C. Volta, *J. Catal.* **1990**, *123*, 417.
249. J. G. Eon, R. Olier, J. C. Volta, *J. Catal.* **1994**, *145*, 318.
250. T. Blasco, A. Galli, J. M. L. Nieto, F. Trifiro, *J. Catal.* **1997**, *169*, 203.
251. P. Concepcion, M. T. Navarro, T. Blasco, J. M. L. Nieto, B. Panzacchi, F. Rey, *Catal. Today* **2004**, *96*, 179.
252. A. A. Lemonidou, L. Nalbandian, I. A. Vasalos, *Catal. Today* **2000**, *61*, 333.
253. M. Machli, E. Heracleous, A. A. Lemonidou, *Appl. Catal. A: General* **2002**, *236*, 23.
254. R. Grabowski, B. Grzybowska, K. Samson, J. Sloczynski, J. Stoch, K. Wcislo, *Appl. Catal. A: General* **1995**, *125*, 129.
255. R. Grabowski, B. Grzybowska, A. Kozlowska, J. Sloczynski, K. Wcislo, Y. Barbaux, *Top. Catal.* **1996**, *3*, 277.
256. A. Galli, J. M. L. Nieto, A. Dejoz, M. I. Vazquez, *Catal. Lett.* **1995**, *34*, 51.

257. J. M. L. Nieto, P. Concepcion, A. Dejoz, F. Melo, H. Knozinger, M. I. Vazquez, *Catal. Today* **2000**, *61*, 361.
258. A. Klisinska, A. Haras, K. Samson, M. Witko, B. Grzybowska, *J. Mol. Catal. A: Chemical* **2004**, *210*, 87.
259. A. Klisinska, S. Loridant, B. Grzybowska, J. Stoch, I. Gressel, *Appl. Catal. A: General* **2006**, *309*, 17.
260. J. Sloczynski, *Appl. Catal. A: General* **1996**, *146*, 401.
261. L. Owens, H. H. Kung, *J. Catal.* **1994**, *148*, 587.
262. K. Aika, M. Kumasaka, T. Oma, O. Kato, H. Matsuda, N. Watanabe, K. Yamazaki, A. Ozaki, T. Onishi, *Appl. Catal.* **1986**, *28*, 57.
263. S. E. Siporin, R. J. Davis, *J. Catal.* **2004**, *225*, 359.
264. K. Aika, T. Takano, S. Murata, *J. Catal.* **1992**, *136*, 126.
265. W. Rarog-Pilecka, E. Miskiewicz, S. Jodzis, J. Petryk, D. Lomot, Z. Kaszkur, Z. Karpinski, Z. Kowalczyk, *J. Catal.* **2006**, *239*, 313.

5.4
Hydrocarbon Reaction Mechanisms

*Don S. Santilli and Bruce C. Gates**

5.4.1
Introduction

The technological importance of surface-catalyzed hydrocarbon reactions has motivated years of effort to understand their mechanisms. However, because of the difficulty of determining surface reaction intermediates, understanding of surface reaction mechanisms lags far behind that of solution reaction mechanisms, and what is known about the former is fragmentary and often largely based on presumed analogies with the latter, combined with results such as those from tracer experiments, kinetics experiments, and theoretical chemistry. The most significant recent progress in understanding of the details of mechanisms of hydrocarbon reactions on surfaces has emerged from theoretical chemistry, which, for example, has helped to distinguish relatively stable reaction intermediates such as alkoxides on catalyst surfaces from transition states in catalytic reactions, such as carbenium ions.

This chapter provides a brief, introductory summary of mechanistic information about hydrocarbon reactions, restricted for brevity to those catalyzed by solid acids or by metals. Related information is presented in the parts of this Handbook dealing with acidity and basicity (Chapters 3.2.4.1 to 3.2.4.4), computer simulation of sorption, diffusion and shape selectivity (Chapters 5.5.2 and 5.5.3), petroleum refining reactions (Chapters 13.5, 13.7, and 13.8), and petrochemical conversions (Chapters 14.3 and 14.4). In addition, various other chapters are concerned with catalysis by acids and metals.

* Corresponding author.

5.4.2
Acid–Base Catalysis

Catalysis by acids and bases generally proceeds via cycles involving hydrogen transfer reactions. In solution, solvent molecules such as water often play a role, for example by interacting strongly with reaction intermediates and/or by being donors or acceptors of protons. Reactions catalyzed by soluble acids or bases are also catalyzed by solid acids or bases, but the solid-catalyzed reactions usually take place in the absence of solvents and at much higher temperatures than are practical with solutions. When solid catalysts incorporate functional groups similar to those of soluble catalysts, there are close analogies between the two. For example, sulfonic acid groups in ion-exchange resins (used to catalyze the synthesis of methyl-*tert*-butyl ether from isobutylene and methanol) act catalytically much like soluble toluenesulfonic acid.

When proton-donor groups are dissociated and hydrated so that (hydrated) H_3O^+ ions are present, then these are the catalytically active species, and the term ''specific acid catalysis'' is applied. Such catalysis is virtually the same in solution and near the surface of a hydrated solid acid such as an ion-exchange resin. Catalysis by OH^- is called ''specific base catalysis''. On the other hand, when undissociated acid (or base) groups are the catalytic sites, the catalysis is called ''general acid (or base) catalysis''. General acid catalysis, whether in solution or on a surface, is usually complex because a variety of unidentified species may be simultaneously present and catalytically active.

General acid catalysis predominates in solid acid catalysis. Because typical solid acids such as metal oxides incorporate both a spectrum of proton-donor groups such as OH groups (Brønsted acid sites) and a spectrum of electron-pair acceptor groups (Lewis acid sites) with various strengths, the catalytic sites often remain unidentified. Thus, although there may be simple relationships between catalytic activity and easily measured properties characterizing acidity, they often do not provide much insight into the nature of the catalytic sites or the reaction mechanism. The same holds true for basicity and catalysis by bases. Thus, the analogies between solution and surface acid (or base) catalysis are for the most part rather weak, and the mechanistic interpretations summarized here are simplified.

5.4.3
Carbocations and Their Reactions

The key reaction intermediates in acid-catalyzed hydrocarbon reactions are carbocations [1–7], the reactions of which are summarized below. Reactions proceeding by radical intermediates are ignored in this chapter, although